Author Contributions:

Conceptualization: C. Sippl, T. John, S. M. Schmalholz
Formal analysis: C. Sippl
Investigation: C. Sippl
Methodology: C. Sippl
Validation: C. Sippl, A. Dielforder, T. John, S. M. Schmalholz
Visualization: C. Sippl, A. Dielforder
Writing – original draft: C. Sippl, A. Dielforder
Writing – review & editing: T. John, S. M. Schmalholz

Global Constraints on Intermediate-Depth Intraslab Stresses From Slab Geometries and Mechanisms of Double Seismic Zone Earthquakes

C. Sippl[1] , A. Dielforder[2] , T. John[3] , and S. M. Schmalholz[4]

[1]Institute of Geophysics, Czech Academy of Sciences, Prague, Czech Republic, [2]Institute of Geology, Leibniz-Universität Hannover, Hannover, Germany, [3]Institute of Geological Sciences, Free University of Berlin, Berlin, Germany, [4]Institute of Earth Sciences, University of Lausanne, Lausanne, Switzerland

Abstract Double seismic zones (DSZs), parallel planes of intermediate-depth earthquakes inside oceanic slabs, have been observed in a number of subduction zones and may be a ubiquitous feature of downgoing oceanic plates. Focal mechanism observations from DSZ earthquakes sample the intraslab stress field at two distinct depth levels within the downgoing lithosphere. A pattern of downdip compressive over downdip extensive events was early on interpreted to indicate an unbending-dominated intraslab stress field. In the present study, we show that the intraslab stress field in the depth range of DSZs is much more variable than previously thought. Compiling DSZ locations and mechanisms from literature, we observe that the "classical" pattern of compressive over extensive events is only observed at about half of the DSZ locations around the globe. The occurrence of extensional mechanisms across both planes accounts for most other regions. To obtain an independent estimate of the bending state of slabs at intermediate depths, we compute (un)bending estimates from slab geometries taken from the slab2 compilation of slab surface depths. We find no clear global prevalence of slab unbending at intermediate depths, and the occurrence of DSZ seismicity does not appear to be limited to regions of slab (un)bending. Focal mechanism observations are frequently inconsistent with (un)bending estimates from slab geometries, which may imply that bending stresses are not always prevalent, and that other stress types such as in-plane tension due to slab pull or shallow compression due to friction along the plate interface may also play an important role.

Plain Language Summary In subduction zones, a plate of oceanic lithosphere descends into the mantle. This means it gets bent from a horizontal orientation offshore the subduction zone to an inclined orientation. Analogous to the bending of a solid beam, this bending of the oceanic lithosphere creates extension in the upper part and compression in the lower part of the oceanic plate. The orientation of these stresses can be retrieved from earthquake focal mechanisms for events that occur in the outer rise region, that is, offshore the actual subduction zone. At deeper depths, downgoing slabs are thought to straighten, which means they decrease their curvature and "unbend." This has the opposite signature in earthquake focal mechanisms as the bending. We compiled focal mechanism information from in-slab earthquakes from global subduction zones, in order to check if such an "unbending" signature is present everywhere at depths of 50–300 km. We find that only about half of the investigated regions show such a signature, while the other ones are extensive everywhere. We then compare these findings with global slab shapes and try to constrain what different processes (e.g., stretching of the entire slab due to its weight, bending forces) influence the stress field inside downgoing plates.

1. Introduction

Subducting slabs of oceanic lithosphere are subject to forces such as slab pull, ridge push, or mantle drag that control the state of stress within the slab (e.g., Buffett, 2006; Capitanio et al., 2009; Forsyth & Uyeda, 1975; Isacks & Molnar, 1969; Ribe, 2001; Schellart, 2004). To first order, the stresses resulting from these forces can be classified into two main types: in-plane (or membrane) stresses and bending stresses (e.g., Medvedev, 2016). While in-plane stresses have a constant sign throughout a slab-perpendicular section, bending stresses resulting from the bending and unbending of a slab vary across the slab and change sign at a neutral plane somewhere between slab surface and bottom (Figure 1; e.g., Craig et al., 2014; Sandiford et al., 2020). The natural processes and their driving forces often cause a combination of in-plane and bending stresses. For instance, slab pull is a
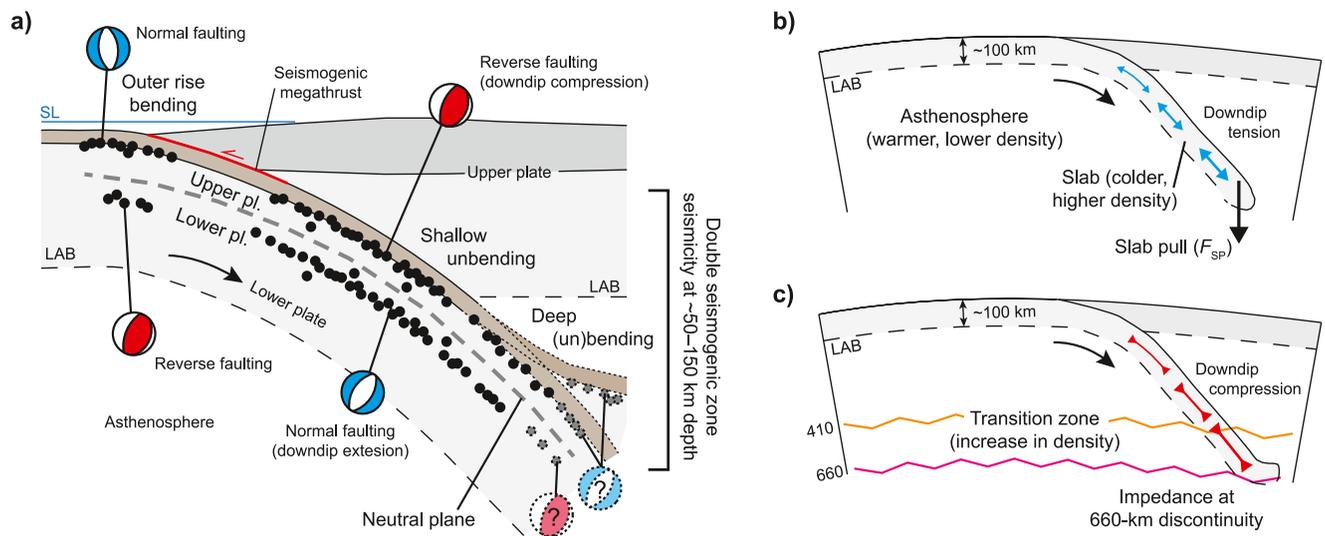
Figure 1. (a) Schematic illustration of double seismic zone (DSZ) seismicity in subduction zones. The two planes of the DSZ are defined by parallel alignments of intraslab earthquakes (black dots). In the outer rise region, the oceanic plate is bent downwards, which leads to extensive focal mechanisms at shallow depth and compressive ones deeper inside the plate. Beyond the megathrust, the slab shape straightens due to unbending, which is thought to cause downdip compression in the upper plane (pl.) and downdip extension in the lower plane. Bending stresses are zero along the neutral plane. At greater depth the slab can be further bent or unbent, as indicated by the dashed slab segments. Whether the deep (un)bending causes a reversal in stress and focal mechanisms is not clear. Note that the displayed focal mechanisms are map view projections of LAB, lithosphere asthenosphere boundary; SL, sea level (b, c) In-plane stresses evoked by slab pull (b, downdip tension) and resistance at the 660-km discontinuity (c, downdip compression).

consequence of the density contrast between the colder and denser slab and the warmer and less dense mantle surrounding it. The density contrast causes a gravitational pull oriented toward the center of the earth, which causes tensile in-plane stresses as well as bending stresses (e.g., Capitanio et al., 2009; Schellart, 2004; Turcotte & Schubert, 2002). In contrast, suction forces exerted by the combination of slab rollback and the presence of thick cratonic lithosphere in the upper plate (Manea et al., 2012) are thought to evoke upward bending, flat slab subduction, and in-plane compression in the shallower part of the slab. In-plane compression is also expected to occur where slabs impinge on or get deflected (bent) at the 660-km discontinuity at the base of the mantle transition zone (see Figure 1c; e.g., Isacks & Molnar, 1971; Goes et al., 2017).

The state of stress inside a slab is difficult to assess directly, but intraslab earthquakes and their focal mechanisms provide valuable hints. In the outer rise region of subduction zones, where the oceanic plate bends and starts to plunge under the overriding plate, focal mechanisms of shallow earthquakes show extension perpendicular to the trench, while rarer small earthquakes at depths of $\geq$20–30 km within the slab show compression perpendicular to the trench (Craig et al., 2014; Gamage et al., 2009; Lefeldt et al., 2009). This signature of extension-over-compression is ubiquitous for outer rise regions around the globe (Craig et al., 2014) and appears as a consequence of downward bending of the slab due to slab pull and the weight of the overriding plate (Figure 1). At intermediate depths, that is, at depths between 50 and 300 km, the situation is less straightforward. The stress field inside subducting slabs at these depths was initially thought to be dominated by in-plane stresses, namely downdip tension due to slab pull and downdip compression of the slab due to the impedance contrast between upper and lower mantle at the 660-km discontinuity (Figures 1b and 1c; Chen et al., 2004; Isacks & Molnar, 1971; Vassiliou & Hager, 1988). Earthquakes at intermediate depths often form double seismic zones (DSZs), alignments of hypocenters along two parallel planes that follow the slab dip and are separated by 15–35 km (e.g., Brudzinski et al., 2007; Florez & Prieto, 2019). Early observations of DSZ seismicity from Japan and Alaska (Engdahl & Scholz, 1977; Fujita & Kanamori, 1981; Hasegawa et al., 1978) revealed opposite kinematics in the two planes of the DSZ, with downdip extension in the lower and downdip compression in the upper plane. The observation of downdip compressive over downdip extensive mechanisms in those DSZs was interpreted as signature of plate unbending, which occurs where the slab curvature acquired by bending in the outer rise region reduces and the slab becomes straight again (see Figure 1a). The observations of plate unbending signatures at intermediate depths led to the proposal of a number of conceptual models of DSZ seismicity creation through plate unbending (Engdahl & Scholz, 1977; Faccenda et al., 2012; Kawakatsu, 1986; Wang, 2002). However, whether

bending/unbending stresses dominate at intermediate depths globally remains uncertain. Global compilations of intraslab focal mechanisms (Alpert et al., 2010; Bailey et al., 2012; Isacks & Molnar, 1971) do not distinguish the two planes of DSZs due to lacking spatial resolution. Moreover, there is much evidence that DSZ seismicity is primarily caused not by intraslab stresses but by dehydration reactions in the slab that are strongly dependent on temperature and hydration state (e.g., Ferrand et al., 2017; Hacker, Abers, & Peacock, 2003; Hacker, Peacock, et al., 2003; Kirby et al., 1996; Peacock, 2001; Yamasaki & Seno, 2003; Zhan, 2020).

To date, most numerical simulations of oceanic subduction (e.g., Babeyko & Sobolev, 2008; Bessat et al., 2020; Faccenda et al., 2012) resemble the characteristics of the NE Japan reference case, that is, a slab that is first bent, then unbent to finally subduct to greater depth in a roughly straight geometry. Recent compilations of slab geometries (Hayes et al., 2018), however, show that most subduction systems feature much more complex geometries than NE Japan, which should lead to different signatures in the DSZ focal mechanisms. A number of local studies (Evanzia et al., 2019; Kao & Rau, 1999; Ratchkovsky et al., 1997; Sippl et al., 2019) as well as in-depth investigations based on globalCMT data (Sandiford et al., 2020) have indeed found evidence for DSZ earthquake focal mechanisms that deviate from a plate unbending signature. Whether these deviations reflect multiple cycles of bending and unbending, a dominance of in-plane stresses or a superposition of different stresses remains unclear.

In this study, we aim to evaluate whether plate unbending signatures typically accompany DSZ seismicity, or if the intraslab stress field is more variable on a global scale. To this end, we first compile global observations of DSZ seismicity from literature and analyze their associated focal mechanism observations (Section 2). We then try to estimate plate bending and unbending from slab geometries using the global slab2 data set of slab surface depths in order to independently constrain the bending state of the different slabs (Section 3). Combining these two strands of observations and conducting a more in-depth look on two very different subduction systems (Northern Chile and NE Japan) for which highly resolved data are available, we finally attempt to discuss the different contributions to the intraslab stress field and their relative magnitudes (Section 4).

2. Compilation of Published DSZ Information

2.1. Where do DSZs Occur?

While it is suspected that DSZs are a general feature of most subduction zones (e.g., Brudzinski et al., 2007), they have only been clearly imaged for selected locations. This is mostly because earthquake catalogs based on global and/or teleseismic recordings commonly lack the location precision necessary for resolving a DSZ. With locally recorded data, clear images of DSZs can be obtained, but local surveys with the required resolution have to date only been conducted in a relatively small proportion of all subduction zone segments. We compiled a literature survey of published evidence for DSZ occurrence around the world, summarized in Figure 2, that we will analyze in the following.

Two global studies are available in which DSZs are inferred at multiple subduction zone segments based either on statistical analysis of the ISC/EHB global catalogs (Brudzinski et al., 2007) or on the analysis of depth phases from teleseismic earthquakes (Florez & Prieto, 2019). Beyond this, there is a wealth of local studies in which DSZs have been imaged either based on locally recorded seismic data or using advanced processing for better depth resolution with teleseismic arrivals (e.g., double-difference relocation, analysis of depth phases). Figure 2 shows all locations where DSZs have been imaged or inferred to date. Detailed information about associated parameters as well as the bibliographic sources are listed in Tables A1 and A2 in the Appendix to this article. We only included studies that imaged DSZs based on the retrieved hypocenter distribution; studies that inferred the existence of a DSZ from the presence of earthquake populations with different focal mechanisms (e.g., Comte & Suárez, 1994; Slancova et al., 2000) were excluded, because focal mechanism signatures of DSZs can vary (see below) and are thus not always good indicators for the presence or absence of a DSZ.

Evidence from local seismic networks (marked L in Table A1) usually shows clearly resolved images of DSZs, whereas images based on global/teleseismic evidence (G/T in Table A1) are commonly more fuzzy. The two global studies (Table A2) only show images for selected areas while postulating DSZs for many more regions for which the evidence is not presented. We will thus treat those as lower-fidelity observations, and will only use observations from local and regional studies (blue in Figure 2) for comparisons with slab bending and unbending estimates (see Section 4). Our compilation shows that DSZs have been reported for all major subduction systems. Only for a number of smaller and/or less well studied slab systems (e.g., Makran, Scotia Arc, Caribbean), no
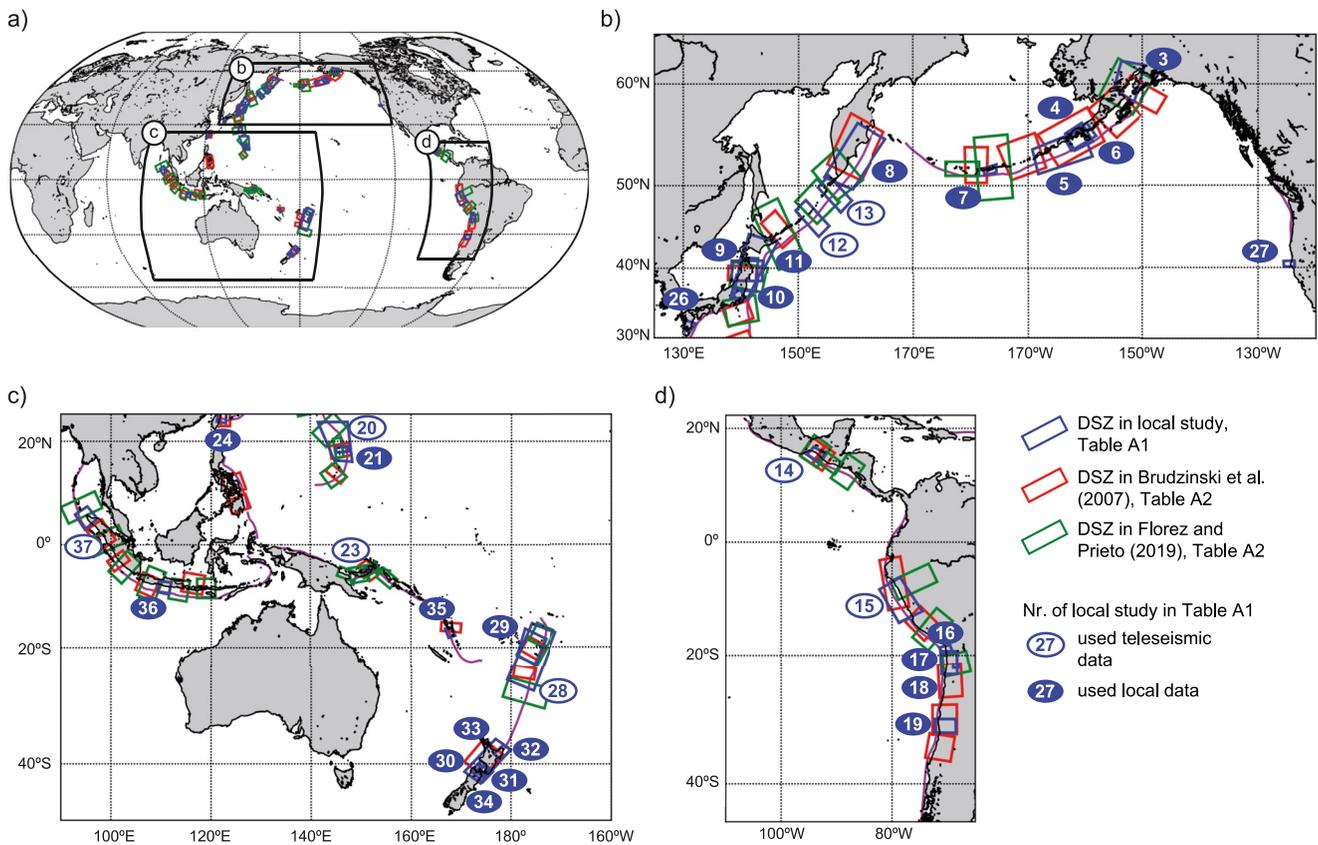
Figure 2. Locations where double seismic zones have been postulated in local studies (blue rectangles) and the global studies of Brudzinski et al. (2007) (red rectangles) and Florez and Prieto (2019) (green rectangles). For details and references, refer to Tables A1 and A2. Magenta solid lines mark trench locations.

observation of a DSZ has been published to date. At the same time, published evidence for DSZs for most larger subduction systems only covers a small proportion of the total along-strike extent of the subduction zone. It is unclear whether the collected DSZ observations approximate where DSZ seismicity actually occurs, or whether the retrieved pattern is mainly a consequence of where high-resolution studies have been carried out to date. It is possible that DSZs are ubiquitous along most subduction systems (as claimed by Brudzinski et al., 2007) and their observation has simply been limited by the availability of local high-resolution data. However, several local studies have reported along-strike transitions between subduction zone segments with and without a DSZ (e.g., Hudnut & Taber, 1987; Nakajima, 2019; Wei et al., 2021), showing that at least some subduction zones do not feature DSZs along their entire length. Since resolution and detection capability are not expected to vary much for the same seismic experiment, these observations clearly demonstrate that there are regions where the lower plane of the DSZ is completely absent. Such a configuration could, for example, be associated with regions of lower and/or shallower hydration of the downgoing oceanic plate (e.g., Geersen et al., 2022).

2.2. Focal Mechanism Observations

Next, we compiled information on the dominant focal mechanisms in the two planes of DSZs from those studies that contained such information (Table A1, Figure 3). The evaluated studies are highly heterogeneous in terms of applied techniques of focal mechanism retrieval, utilized event numbers, as well as the associated uncertainties. The robustness of focal mechanism results depends primarily on the utilized event-station geometry, especially when they are derived from first-motion polarities. Despite the heterogeneous nature of the compiled data set, Figure 3 features consistent clusters, that is, studies located spatially close to each other nearly always show similar results. As previously noted, the vast majority of subduction zone intraslab earthquakes feature either compression or extension oriented subparallel to the downdip direction of the subducting lithosphere. The few cases where neither downdip extension nor downdip compression were observed (labeled "other" in Figure 3)
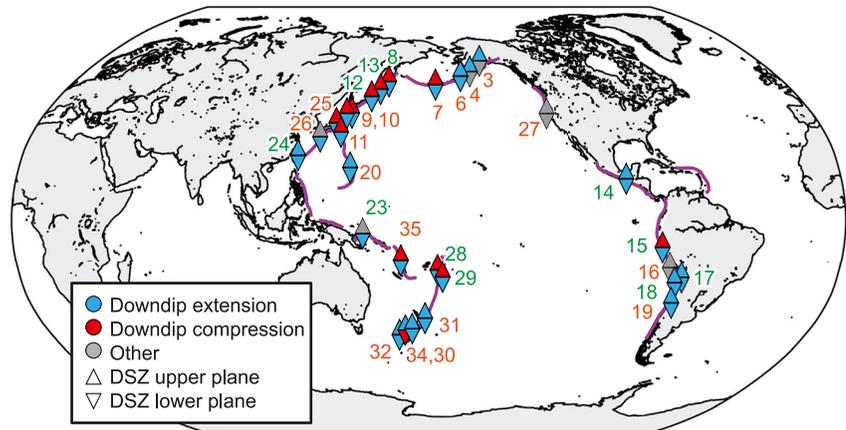
Figure 3. Global survey of focal mechanism data in double seismic zones, numbers next to the symbols refer to the studies listed in Table A1. Orange numbers imply that focal mechanisms were obtained using first motion polarities, green numbers denote studies that used some form of waveform inversion.

likely either indicate inconclusive results that may originate from high uncertainties (e.g., Comte et al., 1999) or a predominance of along-trench orientations because of special regional slab geometries (e.g., Smith et al., 1993).

Our compilation shows that earthquakes in the lower plane of DSZs are downdip extensive nearly everywhere. In contrast, upper plane events are found to be more variable between downdip compression and downdip extension, featuring roughly equal proportions of both of these findings globally (Figure 3). Our compiled observations clearly deviate from the "classical" tenet that DSZs usually have a downdip compressive upper plane over a downdip extensive lower plane, which was largely based on early observations from NE Japan and often interpreted as the signature of slab unbending (e.g., Hasegawa et al., 1978; Kawakatsu, 1986). For those slabs with multiple observations, we observe several cases where the focal mechanism pattern changes along strike of the same subduction system. The Kuril slab that extends from Kamchatka to Eastern Japan is the only larger system that shows a uniform pattern (downdip compressive upper plane over downdip extensive lower plane) along its entire length. The other larger slabs appear to regionally flip between downdip compression and downdip extension in the upper plane along their lengths (e.g., Tonga-Kermadec, South America), while the lower plane is homogeneously extensive. There is a single observation of a compressive lower plane in New Zealand (Evanzia et al., 2019), but other studies located in the direct vicinity have shown extensive upper and lower planes (McGinty et al., 2000; Robinson, 1986). It is unclear whether this implies local-scale variations in the intraslab stress field or possibly not well resolved results. With the exception of two studies in Northern Chile (see Section 4.3), no observations of a systematic change of dominant focal mechanism in direction of slab dip, from downdip compressive to downdip extensive or vice versa, has been reported in literature.

3. Evaluating Slab Geometry

Figure 3 illustrates that global intraslab stress fields in the depth range of DSZs are more variable than has been previously recognized. The "classical" DSZ stress field pattern that is, for example, observed in NE Japan has been widely associated with slab unbending (e.g., Kawakatsu, 1986), while regions that do not show a downdip compressive DSZ upper plane may possess a different intraslab stress field. In an attempt to constrain the current bending or unbending state of the different subduction systems independently from focal mechanism information, we follow Sandiford et al. (2020) and Craig et al. (2022) in taking the current shape of slabs, as provided in the global model slab2 (Hayes et al., 2018), as a proxy for ongoing bending and unbending processes. We use grids of slab surface depth, from which we first calculate slab curvature in downdip direction and eventually derive bending/unbending estimates that we compare with the stress field evidence of Figure 3.
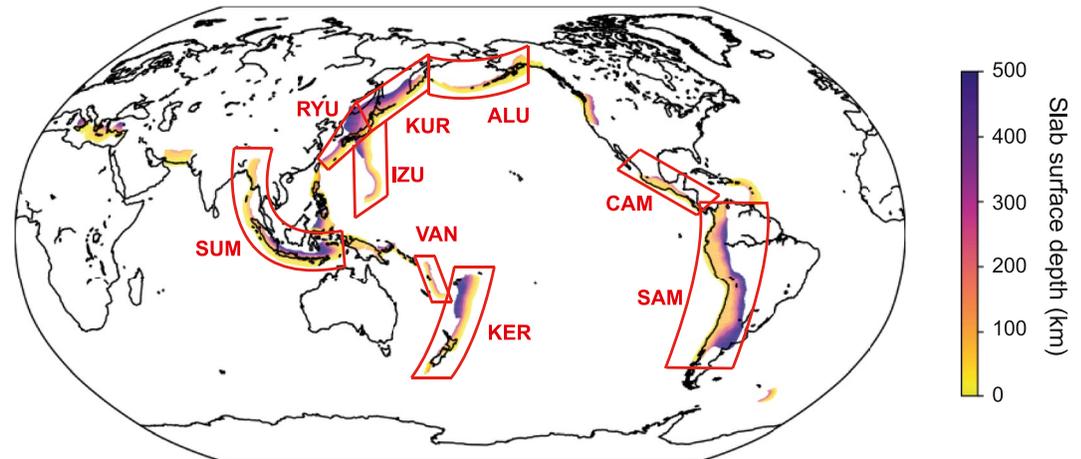
Figure 4. Slab surface depths of all oceanic slabs contained in the slab2 data set (Hayes et al., 2018). The nine large slab systems analyzed in the present study are marked by red frames, and their three-letter abbreviations are given. ALU, Alaska-Aleutian; CAM, Central America; IZU, Izu-Bonin-Mariana; KER, Tonga-Kermadec-Hikurangi; KUR, Japan-Kuril-Kamchatka; RYU, Ryukyu-Nankai; SAM, South America; SUM, Andaman-Sumatra-Sunda; VAN, Vanuatu.

3.1. Data Set

The slab2 data set (Hayes et al., 2018) is a global compilation of interpolated slab surface depths for all seismically active subduction zones (see Figure 4). Slab surface depths are provided on grids with a horizontal spacing of 0.05°, and were interpolated based on a wide variety of published datasets from active seismics, receiver function analysis, the hypocenters of slab earthquakes as well as constraints from seismic tomography. At depths beyond the megathrust, which are most relevant for the present study, the main sources of information are hypocenters of intraslab earthquakes and seismic tomography. Compared to its predecessor slab1.0 (Hayes et al., 2012), additional data and an updated scheme of data synthesis and interpolation should have led to improved 3D slab geometry constraints. In the present study, we only analyze oceanic slabs (thus excluding the continental Himalaya and Pamir-Hindu Kush slabs) and leave out some of the smaller, geometrically more complex and less well-constrained slabs. This leaves us with a data set of the 9 largest subduction systems marked in Figure 4 (South America (SAM), Central America (CAM), Alaska-Aleutian (ALU), Kuril-Kamchatka-Japan (KUR), Ryukyu-Nankai (RYU), Izu-Bonin-Mariana (IZU), Vanuatu (VAN), Tonga-Kermadec-Hikurangi (KER), Andaman-Sumatra-Sunda (SUM)), where the big majority of DSZ observations have been made to date (Figure 2).

3.2. Downdip Plate Curvature

We calculated plate curvature in downdip direction from the slab2 slab surface depth grids by deriving series of trench-perpendicular profiles every 10 km along-strike each subduction zone (see Figure 5; panels I). Along each such profile, we calculated plate curvature as the second along-profile derivative of the slab surface depth, loosely following Buffett and Heuret (2011) and retrieving one data point approximately every 2.5 km along-profile. The results of this calculation are shown in Figure 5 (panels II). Negative values of downdip curvature (visualized as blue areas) denote upward curvature, positive values (red) downward curvature. The retrieved patterns of slab curvature can be complex. The South American slab, for instance, features three bands of (starting from the trench) downward, upward and again downward curvature that take up the uppermost ~200–300 km of the slab (Figure 5a). While the occurrence of these bands is visible nearly everywhere, significant along-strike changes in the downdip width and the magnitude of upward and downward curvature can be seen. The regions of flat slab subduction in Peru and Central Chile can be readily recognized as areas where upward curvature (blue) is distributed over a larger geographical width. The Kuril slab, in contrast, appears much less complex due to its very straight geometry and thus shows only very small deviations from zero curvature (Figure 5c).

Our chosen way of calculating plate curvatures only yields curvature in the downdip direction, with the downdip direction assumed to be perpendicular to the trench. We do not investigate along-strike curvature in this
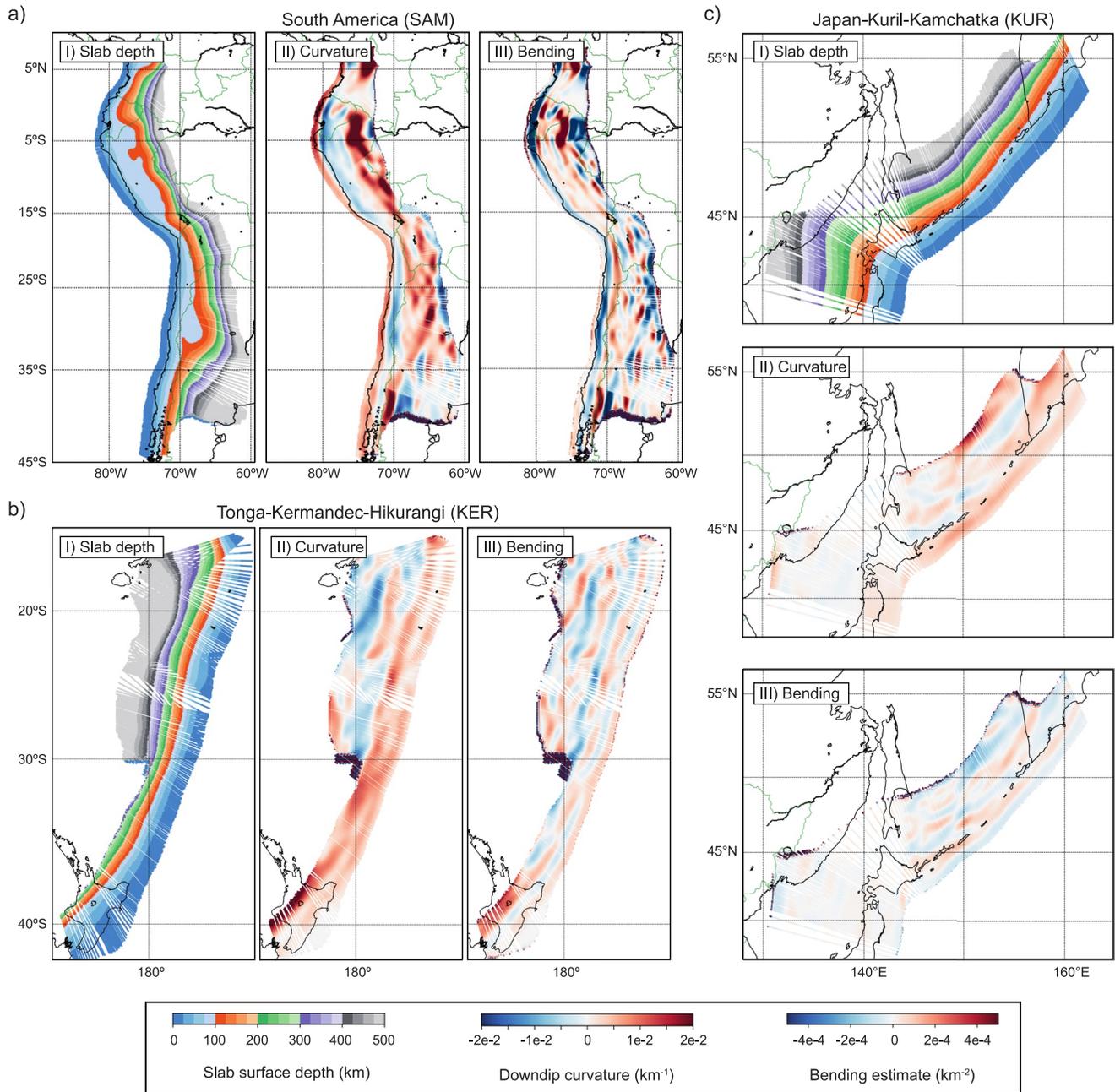
Figure 5. Slab surface depths, downdip curvatures and inferred slab bending/unbending estimates for three selected subduction systems determined from slab2 data. All three properties are shown along the evaluated, trench-perpendicular profiles every 10 km, with along-profile data points about every 2.5 km. Note that negative numbers and blue colors stand for upwards curvature and unbending, whereas positive numbers and red colors represent downward curvature and bending, respectively. For similar plots for the remaining six subduction zones that are shown in Figure 4, please refer to the Supporting Information S1 to this article (Figures S1–S6 in Supporting Information S1).

study, mainly because the global compilation of focal mechanism information (Figure 3) clearly indicates that the intraslab stress field is typically dominated by stresses oriented subparallel to the slab dip direction. There may be exceptions to this rule, as shown by the "other" mechanisms in Figure 3, which may be due to large uncertainties in obtained focal mechanism solutions or to specific local tectonic conditions (such as processes at a slab edge). The largest absolute downdip curvature values encountered for some of the investigated slabs lie around ±0.02 km^{-1}, corresponding to minimal curvature radii of ∼50 km. This value should, however, not be confused with typical curvature radii for subduction zones, which usually fall into the range 300–600 km (e.g., Buffett &

Heuret, 2011). While the latter is the result of fitting a circle sector to the entire smoothed slab shape, what we derive here much more resembles the local "roughness" of the slab's surface.

3.3. Estimating Steady-State Bending/Unbending

The intraslab stress field is partly controlled by plate bending and unbending, that is, the change of plate curvature with time (e.g., Ribe, 2010; Sandiford et al., 2019, 2020). Due to a lack of constraints on past and future slab geometries and their curvatures, we follow other authors (Craig et al., 2022; Sandiford et al., 2020) and estimate plate (un)bending by assuming a "steady state" geometry, that is, we assume that the slab geometry does not change with time. For such a case, the temporal derivative of plate curvature is equivalent to the spatial downdip curvature gradient. Subduction can then be imagined as slab material propagating into the mantle following a fixed trajectory imposed by today's slab geometry. This assumption will be violated where slabs deform rapidly, and there our estimates of slab (un)bending will thus be in error. However, our choice of excluding the smaller, younger and more strongly curved slabs from the analysis and instead focusing on the larger, older and presumably more stable subduction systems (see Section 3.1) should limit this source of misestimation (see also Section 3.4). Estimating steady-state slab bending/unbending in downdip direction for the nine chosen slab systems, we obtain maps of slab bending and unbending (see examples in Figure 5; panels III). We refer to bending as an increase in downward curvature (or decrease in upward curvature) of the slab, and conversely to unbending as an increase in upward curvature (decrease in downward curvature) of the slab.

Our retrieved distributions of (un)bending estimates show considerable complexity for most slabs, exemplified by several trench-parallel bands of bending and unbending in the South American (Figure 5a) and KER slabs (Figure 5b). Bending and unbending estimates for all subduction systems largely fall into the range of ± 0.0005 km^{-2}. The very straight Japan-Kuril-Kamchatka slab (KUR) (Figure 5c) is an exception to this, showing much smaller overall values than all other systems. We will present a detailed analysis of the obtained distributions of slab bending/unbending estimates in Section 4.

3.4. Limitations

The main limitation of our approach is the utilized assumption of a "steady state" subduction process, which may not be valid for all subduction systems that we investigate. If the geometry of a downgoing slab is rapidly changing with time (e.g., during accelerated rollback), there is not necessarily a correspondence between current geometry and bending/unbending stresses (e.g., Spakman & Hall, 2010). Because of the impossibility to derive temporal derivatives of slab geometry, and since a number of previous studies have obtained reasonable results with a similar assumption (Craig et al., 2022; Sandiford et al., 2019, 2020), we nevertheless proceed with this strong assumption and acknowledge that the derived estimates may regionally be in error due to ongoing geometry changes. Since we only investigate the nine largest slab systems on earth and neglect younger, smaller and more strongly curved ones (Figure 4), we likely already exclude most of the slabs where the steady-state assumption is violated. Still, we need to be aware that a retrieved discrepancy between (un)bending estimates from slab geometry and focal mechanism data can simply be a consequence of ongoing slab geometry changes.

A second, less fundamental source of uncertainty in our (un)bending estimates are uncertainties in the slab2 grids of slab surface depth that we used as input to our calculation. These grids are compiled from published hypocenter catalogs as well as seismic tomography studies, hence their uncertainties are directly linked to the amount and quality of such information for each subduction zone. Although a specifically designed consistent methodology was used to derive slab surface depths from tomography information (Portner & Hayes, 2018), we still think that slab2 information is likely less precise in regions where no detailed hypocenter catalogs, preferentially from local seismic networks, are available.

4. Discussion

4.1. Slab Geometries, Curvature, and Bending

In addition to the map view plots provided in Figure 5 (and Figures S1–S6 in Supporting Information S1), we show violin plot representations of slab curvatures (Figures 6a–6c) and bending estimates (Figures 6d–6f) in the depth region of DSZ occurrence for all nine investigated slab systems. Illustrative examples of slab geometry,
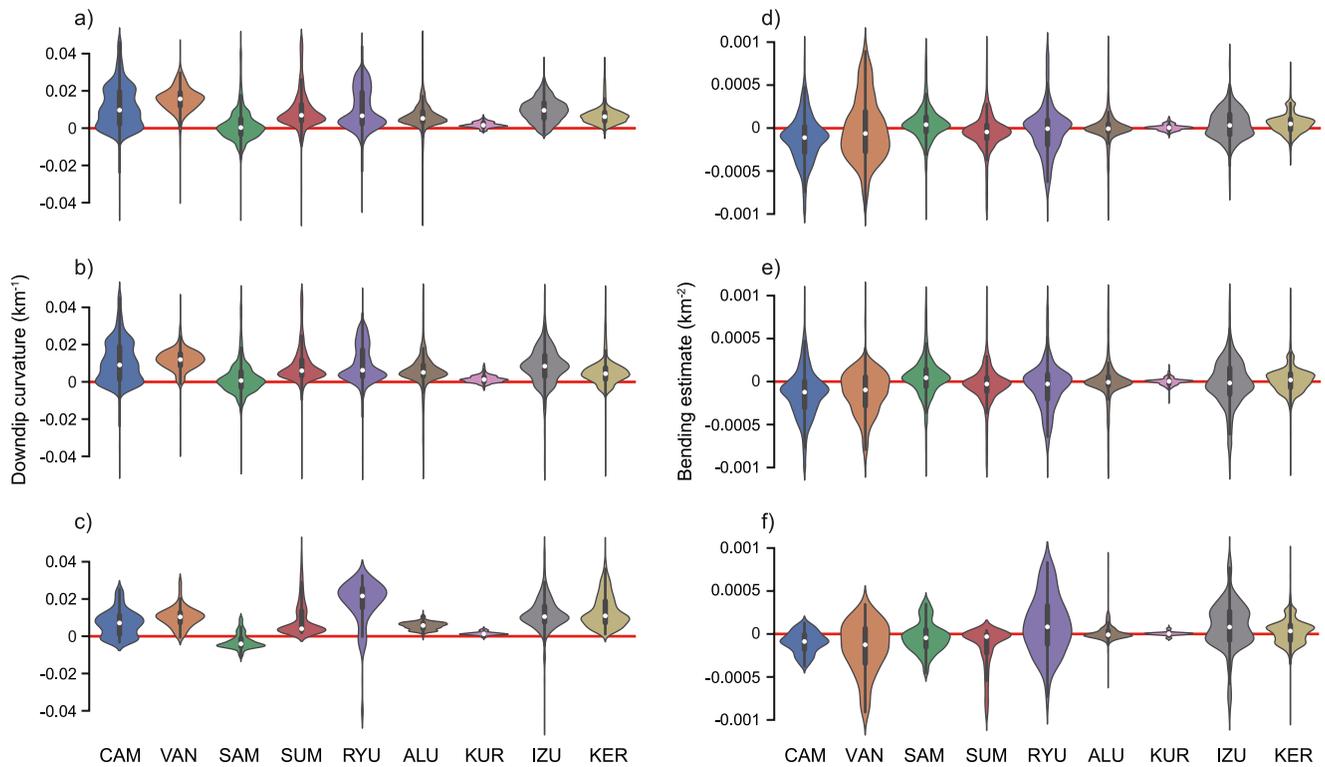
Figure 6. Summary of slab curvature values (left column) and bending estimates (right column) derived from slab2 grids, for different slabs in depth intervals that are associated with double seismic zone (DSZ) seismicity. The violin plots summarize the frequency of occurring curvature data points (negative values correspond to upward curvature, positive values to downward curvature; see Figure 5). The small white dot in the center of each violin is the median of the distribution, the thick black line marks the extent of the inner quartile range, the thin black line extends another 1.5 inner quartile ranges. The outline of the violin shows the entire distribution of the data. Subfigures (a) and (d) show violin plots for the nine slabs in the depth range of 50–150 km. In subfigures (b) and (e), the investigated depth range is the depth range of actual DSZ earthquake observations (see Table A1) in each subduction zone. In subfigures c) and f), finally, only the parts of each slab that fall into the regions of DSZ observations (blue frames in Figure 2) are analyzed, and for each such region the depth range is limited to the depth interval in which DSZ earthquakes have been observed (see Table A1).

curvature and bending for specific regions along the three slab systems shown in Figure 5 are provided in Figure 7. Curvature distributions in the investigated depth range are uniformly shifted to positive values, which indicates a clear prevalence of downward curved slabs. Only the curvature distribution of the South American Slab (SAM) is largely symmetric around zero curvature, and even slightly shifted toward negative values if only the regions of DSZ observations are plotted (Figure 6). This is a consequence of flat slab subduction, where the downgoing lithosphere becomes horizontal again at depths around 100 km, which involves upward curvature of the slab (see examples in Figure 7a). The KUR slab shows only very small, but also dominantly positive curvatures (Figure 6a–6c and 7b), highlighting that this slab is much more straight than all other investigated systems.

The estimates of bending and unbending, that is, the along-dip changes of curvature, show less of a general trend and are largely symmetric around zero (Figures 6d–6f), which implies that they feature both bending- and unbending-dominated areas in the depth interval where DSZ seismicity occurs. While subtle trends with depth can be observed for some of the investigated slabs (Figure 8), those are mostly small in amplitude and rarely involve the entire inner-quartile range of bending values being shifted to one side of the zero line at a specific depth. Although it has a markedly different shape and curvature signature than all other slabs, the bending signature of SAM does not stand out compared to other systems. As already observed for the curvatures, KUR again shows a very narrow distribution of small (un)bending estimates around zero due to its very straight geometry that leads to near-negligible bending estimates.

When exclusively analyzing the areas with confirmed DSZ observations that are marked with blue rectangles in Figure 2, the observed trends slightly change for some of the investigated subduction systems (Figures 6c and 6f), while the overall trends of positive (i.e., downward) curvature and near-zero average bending prevail.
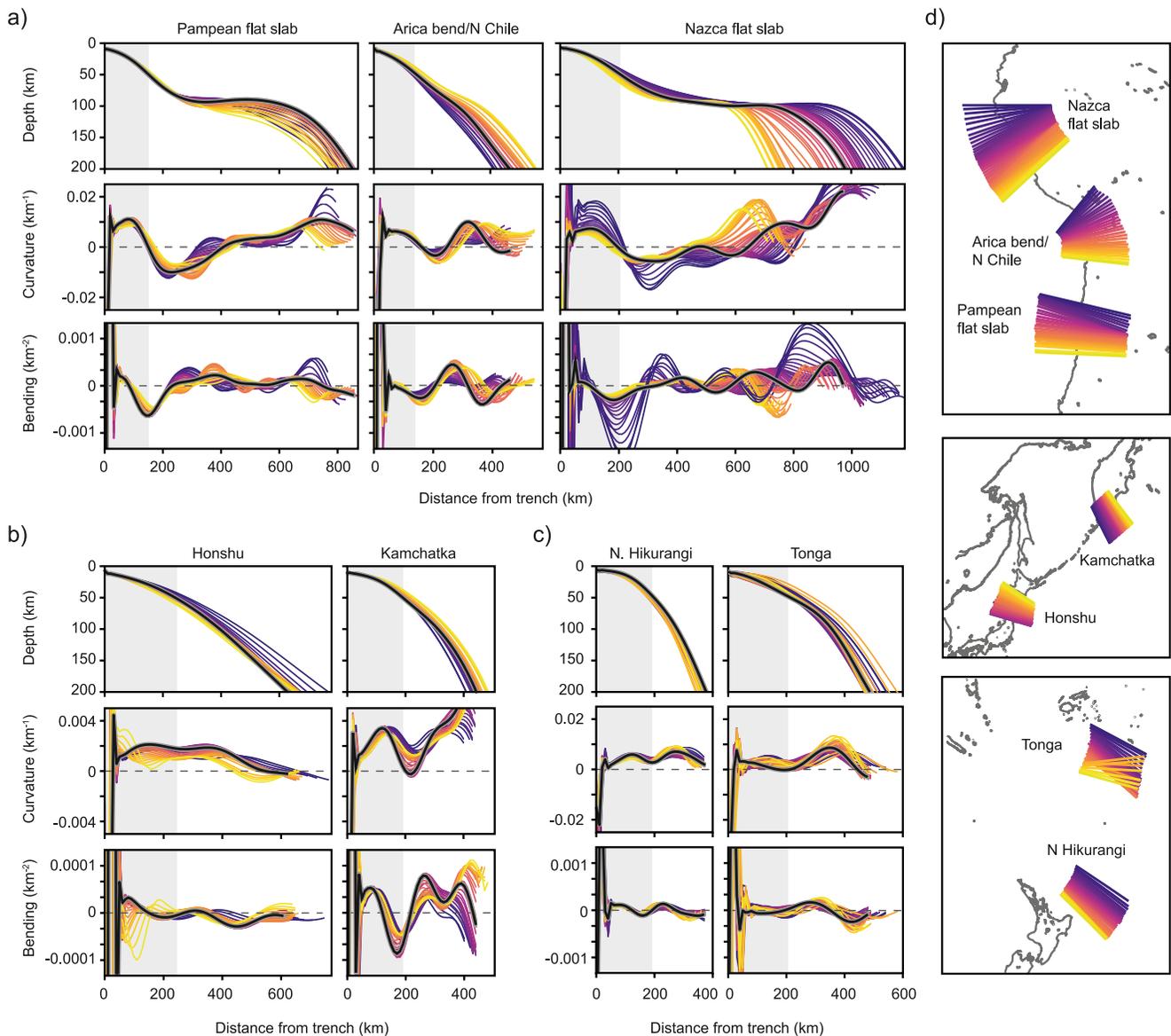
Figure 7. Profiles of slab shape, curvature and bending estimates shown for selected swaths along the South American (a), Japan-Kuril-Kamchatka (b) and Tonga-Kermadec-Hikurangi (c) slabs. Shown are profiles along different swaths (profile position according to color; central profiles of each region shown with thick black lines) in order to capture along-strike variability. For each subfigure, profile positions are shown in (d). Subfigures (a) to (c) consist of two or three columns of slab geometry (uppermost panel), slab curvature (central panel) and slab bending (lowermost panel). Note that the curvature and bending plots for the Japan-Kuril-Kamchatka slab use different scales compared to the other subfigures due to the much smaller values. The gray shading marks the extent of the uppermost 50 km of each slab, which were not sampled by the violin plots in Figure 6.

Notably, regions of DSZ observations in SAM show mostly negative (i.e., upwards) curvatures, whereas the entire slab (Figures 6a and 6b) shows a distribution that is more symmetric around zero. In contrast, the regions with confirmed DSZ seismicity for the RYU slab show clearly stronger downward curvature than the slab average. We thus do not see a specific signature in the curvatures or bending estimates that sets regions with observed DSZ seismicity apart from regions without, or from the entire slabs.

We also investigated whether there are any systematic changes in plate (un)bending with depth. To that end, we subdivided the depth interval 50–150 km into 10 bins of 10 km each, and analyzed the thus aggregated distributions of (un)bending estimates (Figure 8). There is no uniform trend of plate bending or unbending with depth across all subduction zones, the analyzed nine subduction systems rather fall into three different groups with distinct signatures. Group A (Figure 8) comprises the SAM, IZU and KER slabs, and shows a transition from a
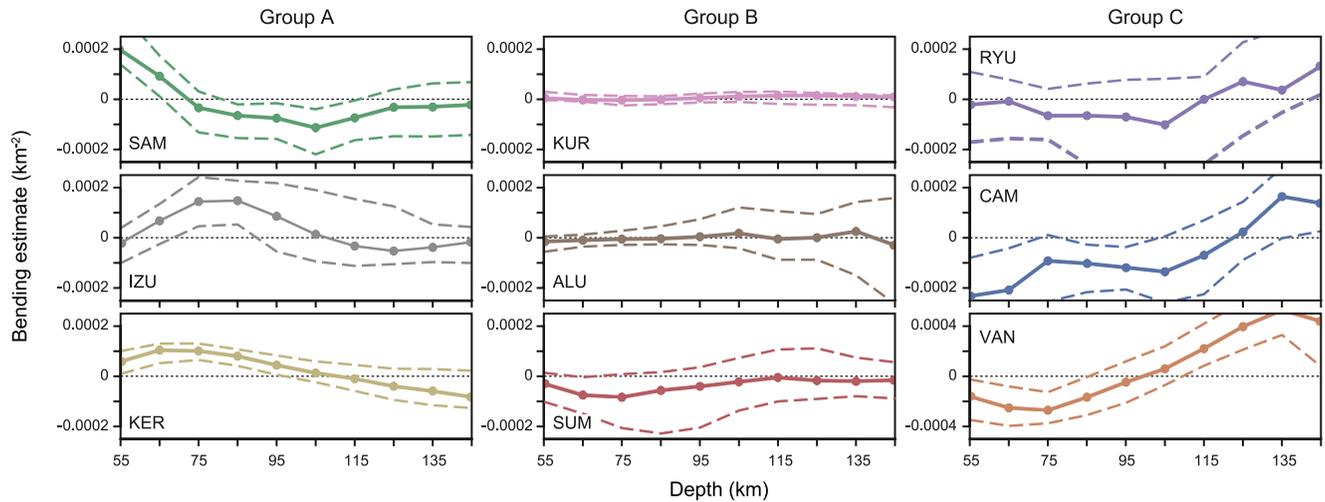
Figure 8. Distribution of bending (values ≥ 0) and unbending (≤0) datapoints in 10 km depth bins in the depth interval 50–150 km for all nine investigated slabs. Shown are the medians of each sub-distribution (solid line, dots) as well as the inner-quartile range (dashed lines). For the abbreviations of the different subduction zones refer to Figure 4, coloring is similar to Figure 6. The results are sorted into three groups: Group A (comprising South America, Izu-Bonin-Mariana and Tonga-Kermadec-Hikurangi) show bending at shallower depth transitioning to deeper unbending, Group C (Ryukyu-Nankai, Central America, Vanuatu) show shallow unbending followed by deeper bending, whereas group B (Japan-Kuril-Kamchatka, Alaska-Aleutian, Andaman-Sumatra-Sunda) shows no trend with depth. Note the different vertical scale for the VAN slab.

bending-dominated shallow part to an unbending-dominated deeper part of the analyzed depth interval. Group B, comprising the KUR, ALU and SUM slabs, shows no clear trend of bending or unbending with depth, and on average features neutral values (with SUM slightly on the side of unbending). A third group (group C; Figure 8), consisting of the RYU, CAM and VAN slabs, shows the opposite trend to group A, progressing from a prevalence of shallow unbending to deeper bending. However, all of these observed deviations from zero (un)bending are small, and in most cases zero (un)bending is contained in the inner-quartile range of the distribution.

These observations are compatible with a pattern of alternating stripes of bending and unbending regions that is already visible in most grids of slab (un)bending estimates (Figure 5; Figures S1–S6 in Supporting Information S1) and shows up more clearly in the profile swaths (Figure 7). Most single profiles show a polarity switch in the (un)bending estimate within the depth range of DSZ seismicity, but since the depth at which this switch occurs often changes along strike, its signature is not very clear in the summed-up depth plots (Figure 8).

4.2. Relation Between Slab Bending, Double Seismic Zone Seismicity, and Intraslab Stresses

Our analysis of slab geometries indicates that for all evaluated slabs the downdip curvature changes on length scales of tens to hundreds of km, which suggests that the slabs experience variable degrees of bending and unbending. The (un)bending of a slab causes bending stresses, whose distribution and magnitudes depend on the mechanical properties of the slab and in particular on its elasticity (e.g., Fourel et al., 2014; Funiciello et al., 2003; Sandiford et al., 2020). The large-scale bending of a slab near the trench area may be considered analogous to the bending of an elastic beam or a thin elastic sheet (e.g., Ribe, 2010; Turcotte & Schubert, 2002), such that the bending stresses increase with distance to a neutral axis that separates the parts of the slab experiencing either tension or compression (Figure 9a). However, for a homogeneous and purely elastic slab, the bending stresses also increase and decrease with curvature, such that unbending beyond the outer rise would simply relax the stresses (Figure 9a), which is at odds with observations of DSZ seismicity (see also Figure 1). The DSZ seismicity beyond the outer rise is therefore understood to reflect bending stresses due to inelastic or permanent (i.e., plastic and/or viscous) deformation of the slab (e.g., Craig et al., 2022; Engdahl & Scholz, 1977; Fourel et al., 2014; Funiciello et al., 2003; Kawakatsu, 1986; Sandiford et al., 2020). Indeed, numerical simulations accounting for an elasto-visco-plastic slab rheology (e.g., Bessat et al., 2020; Sandiford et al., 2020) show that the shallow unbending of the slab causes a reversal from tension to compression in the upper part of the slab and from compression to tension in the deeper part of the slab, in accordance with the classic interpretation of the DSZ seismicity as unbending signature (Figures 1, 9b and 9c).
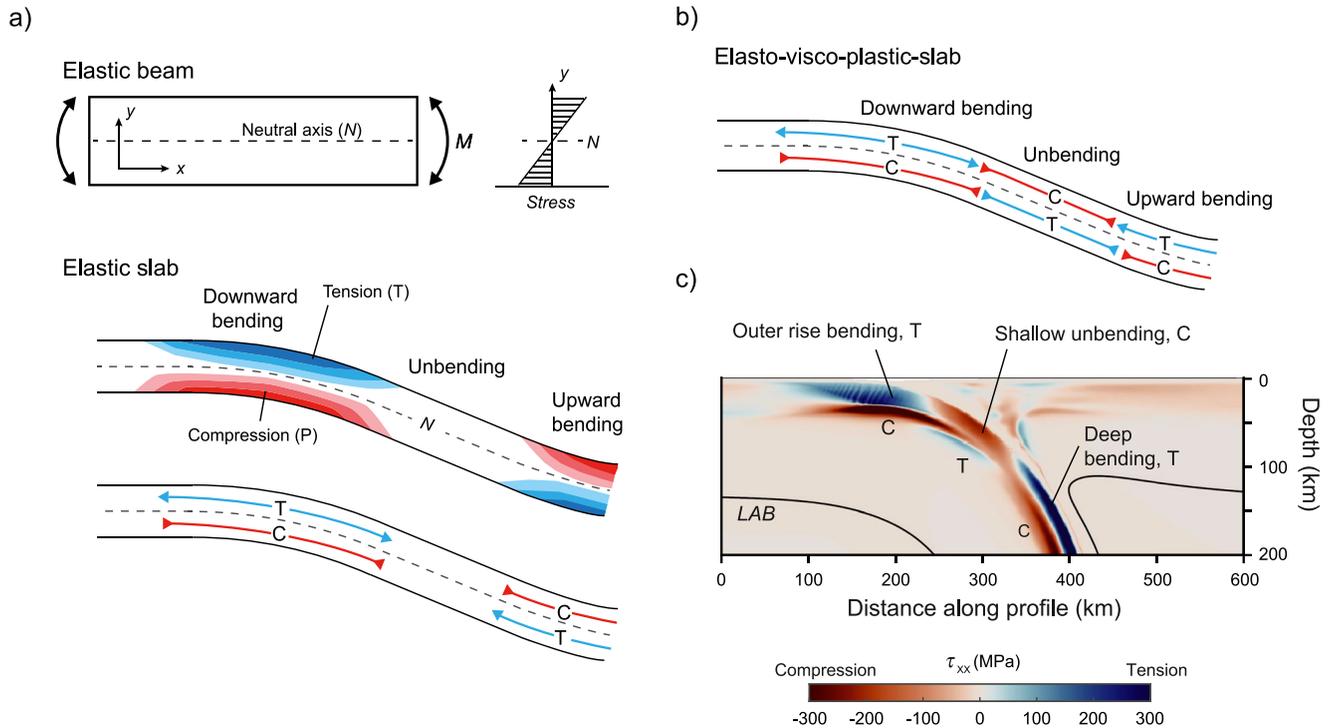
Figure 9. (a) Sketch illustrating the approximation of a slab as an elastic beam. Upward or downward bending of an elastic beam due to a bending moment M causes elastic flexural stresses that linearly increase with distance from the neutral line. For an elastic slab, unbending beyond the outer rise results in a relaxation of stresses. (b) Sketch illustrating the distribution of compression (C) and tension (T) for bending and unbending of an idealized elasto-visco-plastic slab. Note that unbending does not result in stress relaxation as in the elastic case, but a stress reversal. (c) Stress field representation from a numerical modeling study (taken from Bessat et al., 2020), where a transition from outer rise bending to shallow unbending was retrieved, followed by another stress field reversal toward deeper bending at around 120 km depth.

The stress reversals inferred for the shallow unbending area should be also seen at greater depth if the slab experiences additional (un)bending, as schematically shown in Figure 9b (cf. Sandiford et al., 2020). Our compilation of confirmed DSZ seismicity shows, however, no such stress reversals, although the (un)bending estimates indicate that most slabs experience at least one additional switch from unbending to bending or vice versa within the depth range of the DSZ (Figure 8). Instead, we find that the focal mechanisms in the DSZ upper and lower planes remain constant along dip, with the one exception of Northern Chile (see below). Moreover, the DSZ lower planes record almost exclusively downdip tension, while the upper planes record either tension or compression (Figure 3), which raises the question of the extent to which the present-day slab geometry and the DSZ seismicity reflect active slab (un)bending. To address this question, we first evaluate how the (un)bending estimates relate to the DSZ seismicity.

Figure 10 compares the (un)bending estimates derived from the slab2 data set with upper-plane focal mechanisms for regions with confirmed DSZ seismicity. Most distributions of the (un)bending estimates do not deviate far from a zero median and have inner quartile ranges that extend to both sides of the zero line. This dispersion in the (un)bending estimates reflects that the examined sections all feature at least one zero-crossing and related transition from bending to unbending (or vice versa) in the depth range of DSZ as discussed above. This effect is also seen in Figure 6d–6f, 7 and 8. Independently, Figure 10 shows that there is no strong correspondence between the (un)bending estimate and upper-plane focal mechanisms. For example, only 5 of the 8 sections that exhibit a tendency toward unbending record downdip compression in the upper plane (8, 13, 15, 29, 35), while the remaining sections record downdip tension (4, 19, 24). Likewise, regions that exhibit a tendency toward bending show either downdip tension or compression, although there might be a subtle trend toward downdip tension (see 5, 6, 14, 17, 18, 30–34). This trend is also apparent when all sections that feature the same upper plane mechanism type are summed up (Figure 10, inset), although it need not apply to entire slab systems. For instance, the distributions of bending estimates of Sections 28 and 29 (Tonga; see Figure 2) along the KER slab are shifted toward unbending compared to the remainder of sections (30–34; New Zealand) along the same slab system. This is mirrored by the difference in observed focal mechanisms in the upper plane of the DSZ (compressive in 28/29, extensive for
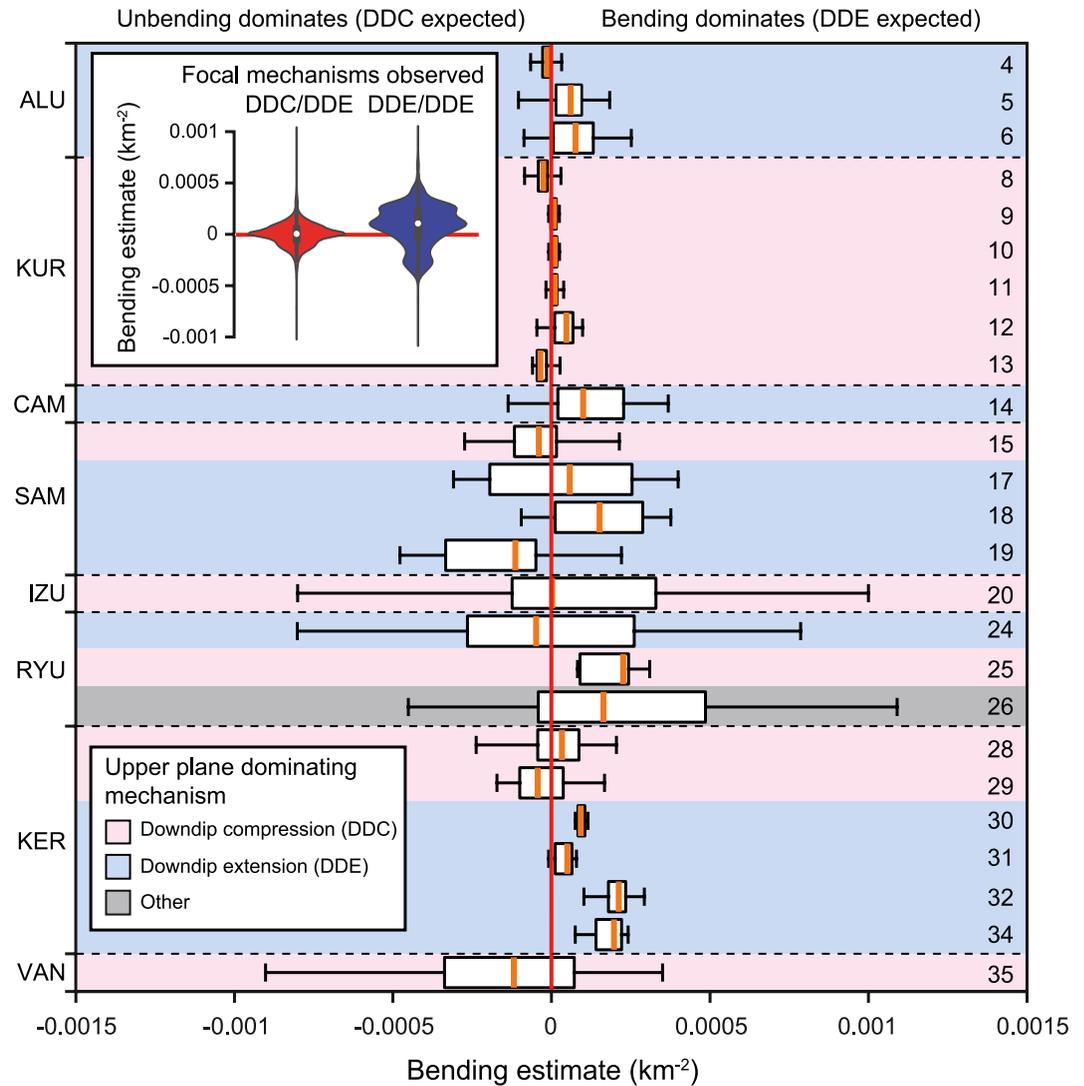
Figure 10. Comparison of focal mechanism information (see Figure 3) to bending estimates for the regions with confirmed Double seismic zone (DSZ) seismicity (Figure 2; Table A2). Shown are boxplots of bending estimates (positive values indicate downward bending, negative values upward bending or "unbending"), in which the orange line represents the median and the white box the inner quartile range of the distribution. The whiskers extend until the furthest data point within another 1.5 inner quartile ranges, outliers are not shown here. Each boxplot represents one region with DSZ and focal mechanism observations, horizontal black lines separate regions belonging to the same slab systems (indicated on the *y*-axis), the numbers on the right refer to the respective studies (see Figures 2 and 3 and Table A2). Red and blue background color marks regions where downdip compressive or downdip extensive upper plane focal mechanisms are observed, respectively. The inset on the upper left shows a comparison of summed slab (un)bending estimates for all regions with downdip compressive over downdip extensive (DDC/DDE) mechanisms and regions where both planes are downdip extensive (DDE/DDE). For an explanation of the violin plot, refer to the caption of Figure 6. The plot shows that while DDC/DDE regions show bending and unbending in about equal parts, the DDE/DDE regions are significantly shifted toward more plate bending.

the rest). For the South American slab, both flat slab regions (Nazca and Pampean Flat Slab; 15 and 19) show a slight unbending dominance, whereas other regions show more bending (17/18). Focal mechanism observations mostly mirror this, except for the Pampean flat slab, where downdip extension was observed (Marot et al., 2013).

The comparison of the (un)bending estimates with the DSZ seismicity suggests that the inferred changes in slab curvature do not condition a specific intraslab stress field. In particular, some of the investigated regions experience downdip tension only and apparently independent of the detailed slab geometry. These findings are difficult to reconcile with a prevalence of bending stresses. In fact, only a minority of the investigated regions (8, 13, 15, 29, 35 in Figure 2) show both a slab geometry and DSZ seismicity consistent with an unbending signature.
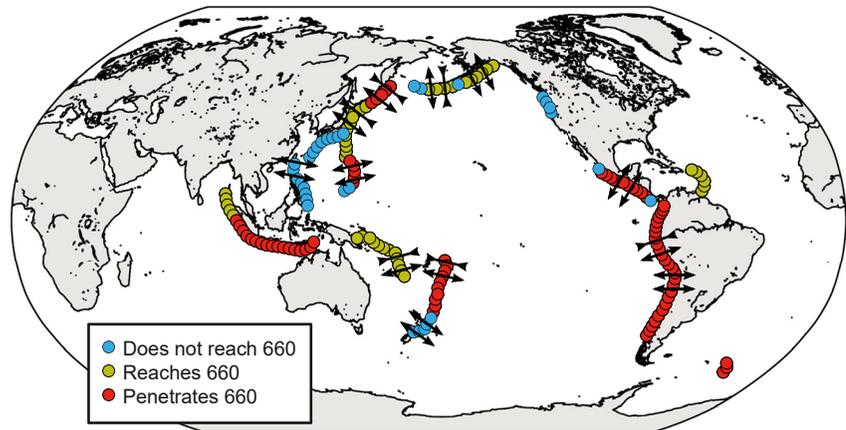
Figure 11. Global compilation of slab extent relative to the 660-km discontinuity, taken from Hu and Gurnis (2020) and based on the tomography models of Li et al. (2008), Obayashi et al. (2013), and Simmons et al. (2012). Intraslab stresses in the double seismic zone, as shown in Figure 3, are plotted on top of the different subduction zones with arrow symbols (two diverging arrows: both planes downdip extensive; converging over diverging arrow: downdip compressive over extensive plane).

We therefore suspect that for many of the investigated slabs the intraslab stress field is currently not dominated by bending stresses, which suggests slab pull or the impedance at the 660-km discontinuity as other potential sources of stress (Figure 1). The majority of studies agrees that at intermediate depths the tension due to slab pull exceeds the compression due to impedance, so that the sum of in-plane stresses is expected to be tensional here (e.g., Craig et al., 2022). A low relative importance of impedance at intermediate depth is consistent with our data compilation, which exhibits no evident correlation between focal mechanisms in the DSZ and the slab extent relative to the 660 km discontinuity, that is, the fault kinematics appear to be not influenced by whether the slab reaches and/or penetrates the 660 km discontinuity (Figure 11, Tables A1 and A2). Figure 11 further shows that the majority of the investigated slabs extend to the 660 or into the lower mantle, and even those that do not still have slab lengths in excess of 300 km, so that the contribution of slab pull (which increases with slab length) should be important. We therefore argue that slab pull is the dominant source of in-plane stresses at intermediate depths and likely conditions the intraslab stress field in regions that exhibit downdip tension only.

Taken together, our analysis of slab geometries and DSZ seismicity suggests that the intraslab stress field may vary significantly at a global scale, with some slabs experiencing mainly in-plane tension but others (un)bending. It should be mentioned, however, that the investigated datasets have limitations that result in some ambiguity. In particular, the lack of resolution and/or insufficient quantity of observations in many studies on DSZ focal mechanisms may imply that possible along-dip changes in focal mechanisms have been missed so far. The slab geometries derived from the slab2 data set include depth uncertainties, which can introduce errors in the inferred (un)bending estimates, although we do not expect any systematic bias due to these uncertainties. Finally, where DSZ seismicity occurs is most likely determined by metamorphic dehydration reactions (e.g., Hacker, Abers, & Peacock, 2003; Hacker, Peacock, et al., 2003; Kirby et al., 1996; Peacock, 2001; Yamasaki & Seno, 2003), which locally cause fluid overpressure and reduce the effective stresses, so that the stress field is sampled only in selected regions that may or may not yield a representative picture of the entire intraslab stress field. Keeping these limitations in mind, we evaluate our findings in the next section for the examples of the DSZs in Northern Chile and NE Japan, for which many uncertainties are reduced due to the available high-resolution data.

4.3. High-Resolution Examples From Chile and Japan

4.3.1. Northern Chile

Our global analysis of plate bending and unbending based on slab2 grids has shown that many subduction zones feature a change from bending to unbending or vice versa within the depth range of DSZ seismicity (Figure 8). A change of DSZ earthquake focal mechanism signature in downdip direction that could correspond to such a change has been, to our knowledge, only shown for the Northern Chile subduction zone to date (Bloch, Schurr,
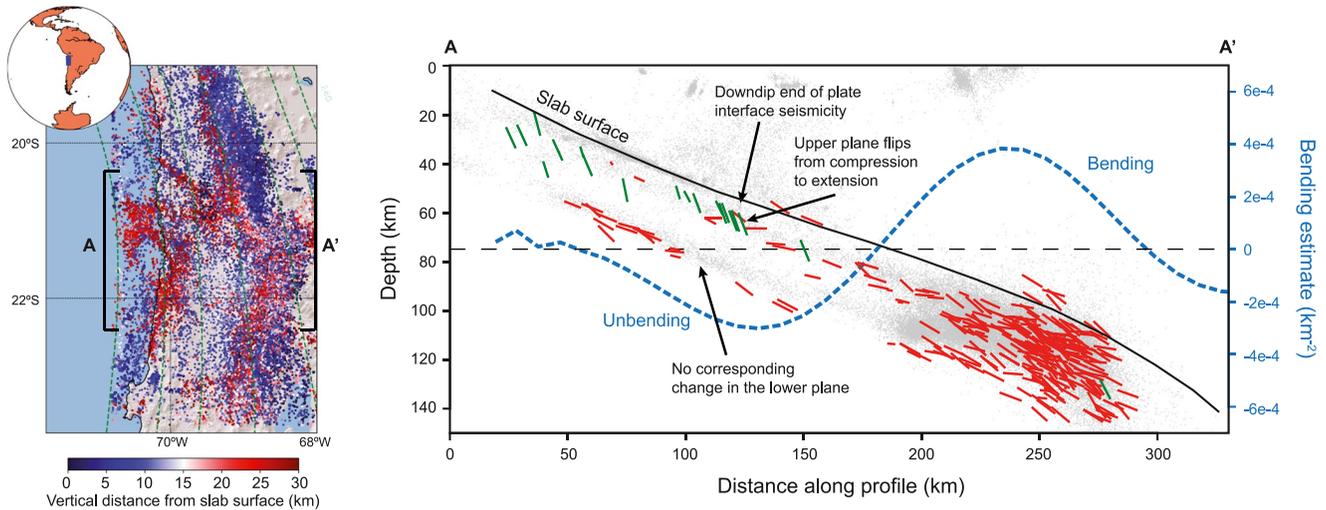
Figure 12. (Left) Earthquake epicenters from the years 2007–2014 taken from the Northern Chile earthquake catalog of Sippl et al. (2018), color-coded by their distance to the slab surface. Blue colors denote upper plane, red colors lower plane events. Black brackets show the swath that is plotted as an E-W profile section in the right subfigure (Right) Intraslab stress orientations in Northern Chile, plotted atop hypocenters from within 1 degree of the profile center at 21.5°S (see left subplot). Red and green bars show the orientation of tensional axes (T axes) of earthquake focal mechanisms from Sippl et al. (2019) within the same swath. Note that the length of each bar indicates whether the T axis is mostly parallel to the profile plane (long bars) or perpendicular to it (point). Green color is chosen when a tensional axis deviates from the slab dip by more than 45°, which is the case when events are downdip compressive. The blue line shows the bending/unbending estimates from the profile through the slab2 data set that is located closest to the shown seismicity cross section (see Figure 5), the black line is the slab surface according to Sippl et al. (2018).

et al., 2018; Sippl et al., 2019). We thus zoom into this subduction zone segment in order to gain a more detailed understanding of the relation between focal mechanisms and (un)bending estimates. Figure 12 shows a W-E profile through the North Chilean subduction zone at 21.5°S. Hypocenters from Sippl et al. (2018) show clearly distinguishable seismicity populations for the upper plate, the plate interface as well as the two planes of the double seismic zone. From a depth of 85–90 km downwards, the two planes of the DSZ disappear, and a highly active, 25–30 km thick cluster of seismicity emerges (Sippl et al., 2019). While earthquakes in this cluster and in the lower plane of the DSZ are uniformly downdip extensive (Figure 12), upper plane earthquakes are compressive at depths shallower than ~55 km and downdip extensive at deeper depths. As has previously been noted by Bloch, Schurr, et al. (2018), the P-axis orientation of these shallow upper plane events is not parallel to the slab dip, but forms an angle of 30–45° relative to the slab surface. A similar transition was also observed by Sandiford et al. (2020) using globalCMT mechanisms that they linked to higher-resolution locations, and interpreted as indicative of the transition from unbending to bending of the slab in this depth range. Our (un)bending grid indeed shows a predominance of unbending around where the compressive mechanisms in the upper plane are observed, and of bending at deeper depths, where T axes uniformly show downdip extension (blue line in Figure 12). However, no mechanism flip in the lower plane is observed where the transition from compressive to downdip extensive mechanisms occurs in the upper plane, as would be expected from a simple change from plate unbending to bending. Some authors (Cabrera et al., 2021; Sandiford et al., 2020) have proposed that a deepening of the stress neutral plane may accompany the change from unbending to bending, so that the entire seismogenic upper ~30 km of the slab are in downdip extension in the deeper part of the slab. Others (e.g., Rietbrock & Waldhauser, 2004) have ascribed the dominance of downdip extensive mechanisms at depths >60 km to strong slab pull.

We think that it is difficult to explain the observations in Northern Chile with the dominance of any one source of stress. If a dominance of bending is invoked, it is difficult to explain why no downdip compressive mechanisms in deeper parts of the slab are observed. While a sudden deepening of the stress neutral plane to depths of >35 km inside the slab can theoretically explain such an observation, we find it an unlikely and rather ad hoc scenario. With the lower plane of seismicity located around the 600–650°C isotherm (Sippl et al., 2019; Wada & Wang, 2009), the proposed location of the neutral plane and especially the downdip compressive part of the slab would be largely situated in the hot and viscous part of the slab, which does not appear to be a mechanically feasible constellation. Moreover, a study on fold structures has shown that rather extreme curvatures are needed

to move the neutral line to the boundary of the bent domain (Frehner, 2011). On the other hand, a prevalence of in-plane tension, possibly as a consequence of slab pull, is hard to reconcile with the presence of compressive events at depths of 35–55 km.

We also note that the sign flip of focal mechanisms in the Northern Chile upper plane coincides remarkably well with the downdip termination of plate interface seismicity (see Figure 12; Bloch, Schurr, et al., 2018; Sippl et al., 2019) and the position of the continental Moho (Yuan et al., 2000). Interplate coupling gives rise to compressive stresses in the vicinity of the plate interface, and the magnitude of coupling should depend mainly on the frictional resistance in the seismogenic zone. The observation that the T-axes are not perpendicular to the slab surface, which implies that P-axes will not be slab-parallel but at an angle of 30–45° to it, is consistent with a horizontal compression of the slab due to friction along the plate interface (Wang & He, 1999). At depths beyond the seismogenic zone, where deformation along the plate interface is dominantly viscous, the stress decreases exponentially and is thought to approach zero at about 80 km depth (Lamb, 2006; Wada & Wang, 2009). Accordingly, the effect of viscous plate coupling is negligible there (Dielforder et al., 2020; Lamb, 2006) and should not affect T-axis orientations. Thus, a compressive contribution of plate interface friction to the intraslab stress field could help to explain the sign flip of the upper plane (transition from plate interface to largely viscous mantle wedge), while it would not affect the consistently extensive lower plane that lies about 20–25 km deeper inside the slab.

4.3.2. NE Japan

Two high-resolution profiles through the Tohoku and Hokkaido parts of the NE Japan subduction zone (Figure 13) show the well-known arrangement of downdip compression over downdip extension first discussed by Hasegawa et al. (1978). Although the dominance of extensive mechanisms in the lower and of compressive mechanisms in the upper plane is clearly visible, there is considerably more scatter in the mechanisms compared to Northern Chile. Despite these local deviations from the compression-over-extension pattern (previously discussed e.g., in Igarashi et al., 2001; Kita et al., 2006; Nakajima et al., 2013), no systematic along-dip change of dominant mechanism signature occurs. The Japan slab is to first order straight at depths beyond ∼60 km, so that inelastic deformation that originates from shallow unbending can be thought to continue to depths of >150 km. Unlike for the Northern Chile case, the position of the stress neutral plane is well known here thanks to the analysis of sparser earthquakes between planes (see dashed red line in Figure 13; Kita et al., 2010). T-axis orientations of the compressive upper plane are perpendicular to the slab surface, unlike in Northern Chile (Section 4.3.1). Since these events are located at depths ≥60 km, that is, beyond the seismogenic zone (e.g., Gao & Wang, 2014; Hayes et al., 2018), a significant contribution of horizontal compression from plate interface friction is not expected here.

The (un)bending estimates we retrieve for the two profiles through the Japan slab are an order of magnitude or more smaller than those for Northern Chile (see Figures 12 and 13). While values along the Tohoku segment are very close to zero for our entire profile, the steeper Hokkaido segment shows a tendency toward (still small) bending values at depths <100 km that is not mirrored in the focal mechanisms. Considering the very small absolute (un)bending values in comparison to other slabs (see also Figures 6d–6f) and their expected uncertainties that will originate in the calculation as well as in the utilized slab model, we can probably only state that the downgoing slab in NE Japan is close to a neutral state between bending and unbending for most of the depth interval we consider here. Given this, it is surprising that an unbending signature in the focal mechanisms indicates that unbending stresses still dominate over in-plane stresses. Possibly, the old and cold Japan slab (about 130 Ma old: see Syracuse et al., 2010) is much more elastic than the Northern Chile one (about 46 Ma old), so that small amounts of (un)bending will still create non-negligible stresses. Whether plate interface stresses contribute to the stress field in the Japan slab, analogous to what we claim for Northern Chile, can not be discerned, because upper plane mechanisms are downdip compressive below the plate interface as well as further downdip (e.g., Gamage et al., 2009).

4.4. Implications for Interaction of Stresses and Absolute Stress Magnitudes

Our analysis of global and local datasets indicates that the stress field at intermediate depth in subducting slabs varies globally and may at different locations be dominated either by bending stresses or tensile in-plane stresses as a consequence of slab pull. The high-resolution datasets from Northern Chile and NE Japan show that the prevalence of a (un)bending signature does not appear to depend on the magnitude of slab (un)bending
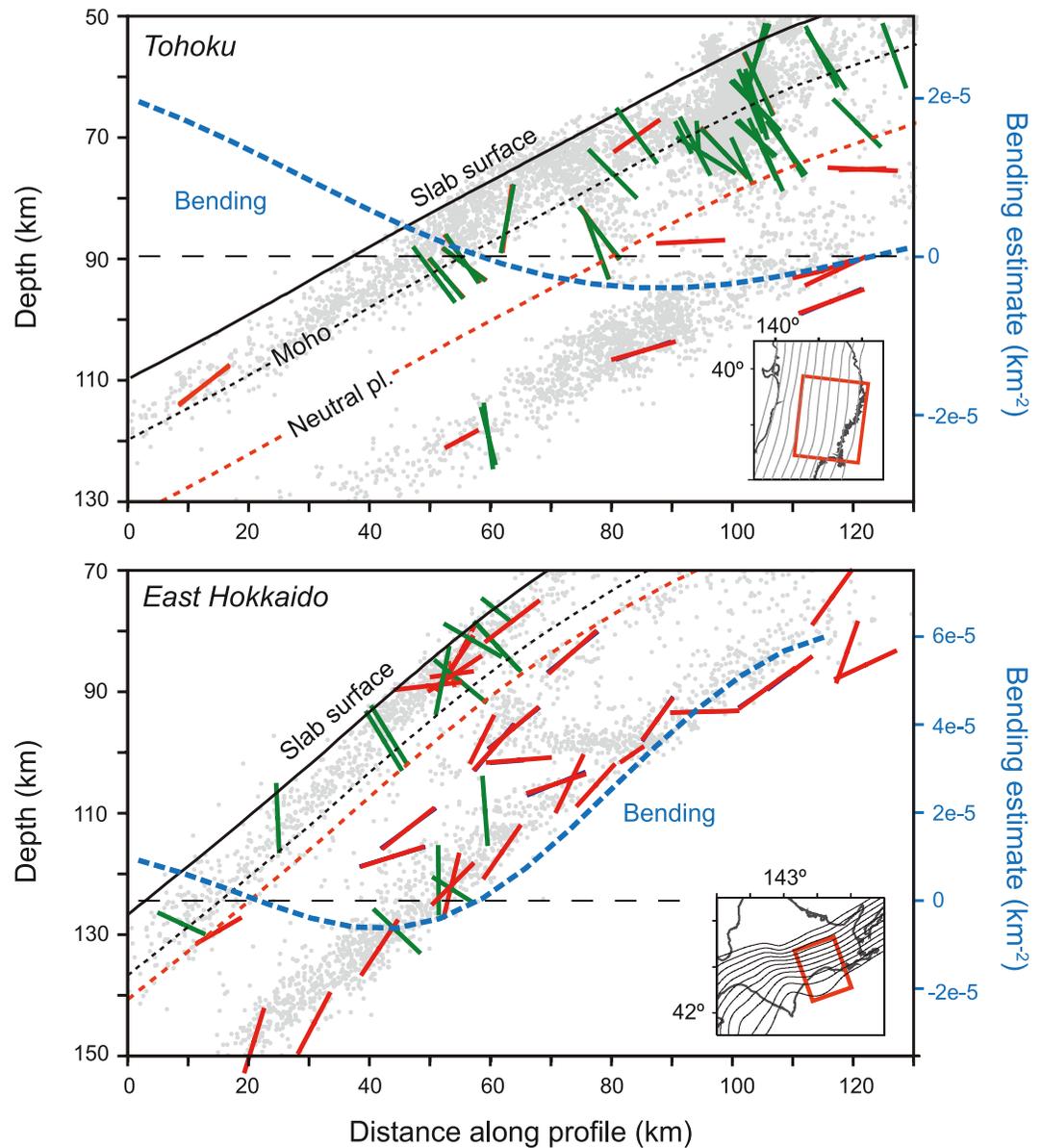
Figure 13. Two trench-perpendicular cross sections through the subducting Japan-Kuril-Kamchatka slab along eastern Honshu/Tohoku (left) and eastern Hokkaido (right), showing T axis orientations and seismicity similar to Figure 12. The profiles are modified from Kita et al. (2010) and show the events located and analyzed therein. As in Figure 12, green T axes deviate from the slab dip by more than 45°, whereas red T axes are aligned with the slab dip (deviation <45°). The blue curve shows (un)bending values estimated from slab2 along profiles located closest to the shown cross sections. The solid black line shows the slab surface, the dashed black line the oceanic Moho and the dashed red line shows the position of the stress neutral plane inferred by Kita et al. (2010).

(Figures 12 and 13). Moreover, the global data compilation shows that a change from slab unbending to bending or vice versa does typically not involve a switch in the dominant focal mechanism in either plane of the DSZ. Only for Northern Chile, a switch in the dominant focal mechanism type in the upper plane of the DSZ is observed at about 55 km depth, which, however, may rather be conditioned by friction along the megathrust. These findings raise the questions of how the processes of slab pull, slab bending and intraplate friction interact and how large the effective stresses that result from this interaction can be.

Absolute stresses resulting from the above processes remain difficult to assess, but our and previous findings allow some constraints as discussed in the following. Numerical subduction models indicate that the pull of the

slab is about $2-3 \times 10^{13}$ N/m in the upper mantle (e.g., Bessat et al., 2020; Erdos et al., 2021), depending on the exact length and density structure of the slab (cf. Turcotte & Schubert, 2002). The downdip tension resulting from slab pull further depends on how much of the force is dissipated by slab bending and slab rollback. The dissipation of slab pull varies mainly with the viscosity contrast between the slab and the mantle and the slab rheology and has been differently estimated with values ranging from as high as 80%–90% (e.g., Bellahsen et al., 2005; Schellart, 2004) to as low as 10%–20% (e.g., Capitanio et al., 2009; Wu et al., 2008). These estimates provide a lower and upper bound for the downdip tension due to slab pull of a few tens of MPa and a few hundreds of MPa, respectively, assuming that the slab pull acts within the upper 50 km of the lithosphere. For comparison, the magnitude of bending stresses can be estimated from the radius of curvature and elastic modulus of the slab (e.g., Fourel et al., 2014; Turcotte & Schubert, 2002). Given that the elastic modulus of rocks is typically about some tens of GPa, the inferred minimal curvature radii of ∼50–100 km translate to elastic bending stresses of several hundred MPa.

The deviatoric stresses due to downdip tension and slab bending may be further limited by the relaxation of stresses by brittle and viscous deformation. In particular, the effective frictional strength of the slab has a great impact on the absolute stress magnitudes that can be sustained. For instance, numerical simulations of oceanic subduction accounting for elasto-visco-plastic deformation indicate that a reduction of the coefficient of friction of the slab from about 0.6 to 0.09 reduces the maximum deviatoric stresses in the slab from a few hundreds to some tens of MPa (Bessat et al., 2020). Especially high elastic bending stresses resulting from small curvature radii may be therefore limited by the effective frictional strength of the slab. However, numerical simulations also indicate that applying a low friction coefficient to the entire slab reduces the strength of the slab so much that it cannot sustain the slab pull anymore, which causes slab breakoff and a termination of subduction (Bessat et al., 2020). In this respect, substantial weakening of the slab and related stress relaxation should be spatially and perhaps temporally restricted and do not affect entire slabs.

The high-resolution data set for Northern Chile shows a dominance of downdip tension except for the DSZ upper plane directly beneath the megathrust. Given our above estimates, the downdip tension may relate to deviatoric stresses of tens to hundreds of MPa. If shearing along the megathrust reverses the state of stress and conditions the observed downdip compression, then the stress on the megathrust must exceed the downdip tension. Previous estimates of megathrust shear stresses based on force-balance and rheological models (Dielforder et al., 2020; Lamb, 2006) indicate for the Andean megathrust deviatoric stresses of about 70–120 MPa at 35–55 km depth (i.e., the depth range for which downdip compression in the DSZ upper plane is observed). It should be noted that these stress estimates represent an average over several subduction earthquake cycles and that current stresses may be slightly higher, especially as Northern Chile is in the late stage of the interseismic period. However, as subduction megathrusts appear to be chronically weak (e.g., Dielforder, 2017; Lambert et al., 2021; Wang et al., 2019), the above estimate of megathrust stresses can be considered representative. Accordingly, megathrust stresses of ∼100 MPa imply that the downdip tension due to slab pull should not exceed some tens of MPa at least in the direct vicinity of the plate interface where downdip compression is observed. Moreover, the effective frictional strength of the faulted rocks must be low enough to allow frictional deformation at deviatoric stresses of some tens of MPa. For the given depth range, this requires an effective friction coefficient of 0.05 or less. As discussed above, such a low effective frictional strength applied to the entire slab would likely cause slab breakoff and terminate subduction. We therefore suspect that the very low strength is spatially restricted to the direct vicinity of DSZ seismicity.

The apparent low-stress and strength conditions inferred for Northern Chile may reflect the impact of different factors and processes. The bending of the oceanic slab in the outer rise region causes large-scale faulting and hydration of the slab due to partial serpentinization of the oceanic lithosphere (e.g., Bostock et al., 2002; Cai et al., 2018; Ranero & Sallarès, 2004). The initial bending, deformation, and alteration of slabs have been shown to drastically reduce their elastic thickness and to frictionally weaken them, at least locally (Arnulf et al., 2022; Craig et al., 2014; Garcia et al., 2019; Hunter & Watts, 2016). With ongoing subduction, the serpentinized slabs dehydrate again. Fluids liberated by dehydration reactions tend to channelize (e.g., Bloch, John, et al., 2018; Plümper et al., 2017) which supports a local pore fluid pressure increase, which can reduce the effective stresses and frictional rock strength and may represent one of the key triggers of DSZ seismicity (e.g., Ferrand et al., 2017; Hacker, Abers, & Peacock, 2003; Peacock, 2001).

While the above arguments can explain the observations from Northern Chile, they cannot explain the global variability in the occurrence of bending and slab pull signatures. Our analysis and findings do not allow resolving this aspect, but we tentatively argue that the global differences may indicate that at the timescale of observation (i.e., years to tens of years), subducting slabs may not experience active (un)bending or the related strain rates are too low to result in relevant stresses. In detail, we argue that there may be no substantial underthrusting or subduction of the slab in-between great megathrust earthquakes, implying that there is no new material that needs to be bent. If slabs are indeed frictionally weakened within the range of the DSZ, the elastic thickness of the slab is substantially reduced (cf. Garcia et al., 2019; Hunter & Watts, 2016). The elastic core may still support the larger-scale bending of the slab in the outer rise region. In the DSZ, however, a low effective strength may allow a relaxation of bending stresses, such that downdip tension due to slab pull prevails. A relaxation of bending stresses may also explain why the intensity of bending, as reflected in the bending estimates, does not determine whether or not the slab shows a bending signature and why almost all slabs show no reversal from downdip compression to tension or vice versa within either plane of the DSZ. In this respect, the state of stress in subducting slabs should be transient on the timescale of the subduction earthquake cycle. The detailed snapshot from Northern Chile may be therefore not representative for the longer-term stress conditions in this or other slabs. We note, however, that our tentative interpretation does not explain the state of stress in individual slabs and that our observations and inferences may be explained otherwise. Whether a short-term relaxation of bending stresses may give prevalence to downdip tension may be evaluated by means of numerical simulations that are capable of resolving subduction zone dynamics on timescales of years to decades.

4.5. Link to Fluid Processes in the Slab

Whereas early studies proposed that DSZ earthquakes occur due to unbending stresses in the slab (e.g., Engdahl & Scholz, 1977; Kawakatsu, 1986), there is nowadays a broad consensus that dehydration reactions occurring inside the slab during its descent while it gets exposed to ever higher temperatures are ultimately linked to the creation of DSZs (Hacker, Peacock, et al., 2003; Kirby et al., 1996), although the exact mechanism of earthquake generation is still unclear (Ferrand et al., 2017; Incel et al., 2017; John et al., 2009; Jung et al., 2004; Zhan, 2020). The hydrous minerals in the slab that break down during prograde metamorphic reactions are formed when water infiltrates into the slab prior to subduction at mid-oceanic ridges, along hotspot tracks (e.g., Seno & Yamanaka, 1996) and, most prominently, at the outer rise of subduction zones, where plate bending leads to the creation of normal faults that penetrate deep into the oceanic plate (Cai et al., 2018; Grevemeyer et al., 2018; Ranero et al., 2005). Taken together with the observation that some intraslab seismicity in Japan even occurs in the direct vicinity of the stress-neutral plane (Kita et al., 2010), this implies that most likely plate hydration and pressure-temperature conditions define where seismicity occurs, whereas the state of stress (downdip compression or extension) plays no major role. Focal mechanisms of DSZ seismicity then image the intraslab stress field that is present where they were created.

While there is likely no significance/large influence of the state of stress on the creation of DSZ seismicity, the processes responsible for generating DSZ seismicity may well influence the intraslab stress field. As mentioned above, liberated fluids from dehydration reactions co-located with DSZ seismicity will locally decrease rock strength in the slab. Field evidence from exhumed high-pressure rocks suggests that such weakening is not permanent but rather occurs in transients (e.g., Austrheim, 1987; Kaatz et al., 2021; Zertani et al., 2019). The slab may thus be substantially weaker, at least for certain time periods, where seismicity occurs and where the slab is affected by fluid-induced transformation processes, whereas the volume between the planes of the DSZ (the cold "elastic core") may remain strong. This could allow stresses that are nominally too weak to be dominant given the overall slab strength to still control the focal mechanism signature of DSZ seismicity. For the Northern Chile case (Figure 12), where seismicity is observed to occur throughout the slab from a depth of about 100 km downwards, the seismicity geometry would imply wholesale, although possibly only transient, weakening of the slab. Such a weakened region in a slab would temporally "decouple" the shallow slab from the slab pull exerted by deeper segments, which may explain the geometry of the Northern Chile slab (shallow flattening, then steepening beyond the possibly weakened segment). Recently presented instrumental evidence (Bedford et al., 2020; Bouih et al., 2022) also hints at such transient episodes of slab weakening. We can not resolve such local and possibly transient changes in slab strength with our analysis, which only considers the geologically current situation. They may, however, represent one potential explanation for our observed misfit between slab geometries and stress field estimates (see above).

A further implication of our work is connected to the question of how deep hydration of the slab can be achieved. A direct relationship between deep hydration of the downgoing slab and DSZ seismicity appears likely (e.g., Geersen et al., 2022; Kirby et al., 1996; Kita et al., 2006; Peacock, 2001), but whether such deep hydration can be acquired in the outer rise regions remains somewhat contentious (Korenaga, 2017). While a mechanism to create fluid pathways during serpentinization and thus facilitate deep hydration has been proposed (Plümper et al., 2012), Faccenda et al. (2012) have suggested an alternative mechanism of deep hydration in which the intraslab stress field acts as a "pumping mechanism" (see also Faccenda and Mancktelow. (2010)) during slab unbending. According to this hypothesis, water that gets released in the compressive upper part could be sucked into the tensile deeper parts of the slab. Given our observations of globally variable intraslab stress fields (Figure 3), we doubt that such a mechanism can explain all occurrences of DSZ seismicity. While an extensive lower seismicity plane that could promote suction of free fluids is indeed near-ubiquitous, the proposed pumping also relies on compressive stresses in shallower parts of the slab that release and drive away fluids. Such compressive stresses in the upper plane appear to be absent in about half of the subduction zones around the globe. We thus believe that such a mechanism, if present, should be of minor importance in most settings.

5. Conclusions

We compiled focal mechanism information from global observations of DSZ seismicity as well as estimates of global slab (un)bending deduced from current geometries (slab2 models). Analyzing and comparing the retrieved datasets, we arrive at the following conclusions:

1. Focal mechanism patterns in DSZs are more variable than previously assumed. While nearly all subduction segments in our compilation feature a downdip extensive DSZ lower plane, DSZ upper planes are downdip extensive or downdip compressive to about equal parts. At the same time, estimates of slab (un)bending from current geometries show distributions that are mostly symmetric around zero for intermediate depths, and only a weak correlation with observed focal mechanisms.
2. An in-depth look onto focal mechanisms and bending estimated from the Northern Chile and NE Japan subduction zones shows that in both cases, the observed stress field is not a simple consequence of the current slab geometry. In Northern Chile, the predominance of downdip extensive mechanisms at deeper depths can not easily be explained with bending stresses and instead suggests a prevalence of in-plane tension due to slab pull. At shallower depth, the upper plane of the DSZ flips to compressive mechanisms around where the plate interface terminates, which strongly suggests a contribution of compressive stress from plate interface friction. In NE Japan, downdip compression in the upper and downdip extension in the lower plane describe a signature of plate unbending, although estimates of plate bending stresses from the current slab geometry are very small and do not clearly show a prevalence of unbending throughout most of the investigated depth range.
3. These observations imply that bending stresses, in-plane tension due to slab pull and compression due to plate interface friction should have comparable magnitudes in most settings. This may imply that downgoing oceanic slabs possess relatively low mechanical strength where DSZ seismicity occurs, which could be a result of ongoing dehydration reactions that promote slab weakening. The incompatibility of focal mechanism observations and current geometries may also arise from changes in slab dynamics and strength that could occur over short timescales, for instance forced by the seismic cycle.
4. Lastly, our observations of variable stress fields throughout different slabs imply that a causal connection of DSZ seismicity to plate unbending, for example, with plate unbending enabling deep hydration of the downgoing plate, can likely not explain all our observations.

In order to better understand the intraslab stress field at intermediate depths in the future, it may be beneficial to perform numerical simulations with time steps that can resolve a single seismic cycle, which is only rarely done to date (e.g., Sobolev & Muldashev, 2017; van Zelst et al., 2019). At the same time, more detailed observational studies of DSZ earthquakes and their focal mechanisms across different subduction zones could reveal whether along-dip changes in mechanism orientation like the one in Northern Chile can be observed elsewhere. A broader observational base of high-resolution studies would provide valuable constraints on the different stress sources and their relative magnitudes in a variety of settings.

Appendix A: Tables of DSZ Occurrences Shown in Figure 2

The following two tables contain the literatur-ederived data that is visualized in Figures 2 and 3, as well as the corresponding bibliographical references.

Table A1
Locations of Double Seismic Zones Postulated in Literature (Local and Regional Studies)

Slab	Region	Coordinates	Depth [km]	Mech UP/LP	660	Source	Data	No.
Alaska-Aleutian	Cook Inlet	61.54/−149.53, 61.90/−153.84 59.61/−155.10, 58.43/−151.65	57–138	DDE/other	R	Ratchkovsky et al. (1997)	L	3
	Shumagin Islands	56.47/−159.87, 55.05/−163.80 53.74/−162.47, 55.21/−158.22	66–125	DDE/other	R	Reyners and Coles (1982)	L	4
	E Aleutians	55.83/−160.67, 53.14/−158.84 51.27/−168.23, 53.85/−169.28	51–119	–	R	Hudnut and Taber (1987)	L	5
	E Aleutians	56.47/−160.71, 54.65/−158.76 53.74/−161.95, 55.43/−163.57	64–148	DDE/DDE	R	Abers (1992)	L	6
	C Aleutians	52.29/−175.52, 51.45/−175.49 51.14/−177.55, 51.88/−177.75	117–195	DDC/DDE	R	Engdahl and Scholz (1977)	L	7
Japan-Kuril-Kamchatka	Kamchatka	56.45/160.21, 54.89/165.18 49.58/159.38, 50.92/154.44	59–164	DDC/DDE	P	Gorbatov et al. (1994)	L	8
	Honshu	40.99/138.40, 37.98/138.48 37.98/143.72, 40.98/143.90	60–160	DDC/DDE	R	Hasegawa et al. (1978)	L	9
	Honshu	36.90/139.03, 41.40/139.96 41.29/142.95, 36.55/142.62	75–171	DDC/DDE	R	Igarashi et al. (2001)	L	10
	Japan Trench	35.74/138.25, 35.55/141.17 43.31/146.32, 44.35/141.39	77–192	DDC/DDE	R	Kita et al. (2010)	L	11
	Kurils	48.37/151.23, 45.36/155.30 44.04/153.47, 47.17/149.48	80–143	DDC/DDE	P	Kao and Chen (1995)	T	12
	Kurils	51.13/155.18, 48.31/159.21 46.96/157.30, 49.78/153.35	80–143	DDC/DDE	P	Kao and Chen (1995)	T	13
Central America	Chiapas	16.89/−94.12, 15.76/−91.98 14.38/−93.66, 15.53/−95.33	47–142	DDE/DDE	P	Zhang et al. (2019)	T	14
South America	S Peru	−8.51/−82.29, −14.36/−78.77 −12.39/−74.54, −6.34/−78.56	50–80	DDC/DDE	P	Isacks and Barazangi (1977)	T	15
	N Chile	−18.60/−71.41, −19.74/−70.94 −19.39/−69.08, −18.19/−69.56	101–165	Heterogeneous	P	Comte et al. (1999) Dorbath et al. (2008)	L	16
	N Chile	−19.26/−71.29, −19.26/−68.29 −23.31/−68.25, −23.30/−71.08	42–105	DDE/DDE	P	Sippl et al. (2018) Sippl et al. (2019)	L	17
	N Chile	−21.49/−68.99, −21.47/−68.00 −22.17/−67.99, −22.19/−68.99	90–120	DDE/DDE	P	Rietbrock and Waldhauser (2004)	L	18
	C Chile	−30.49/−72.30, −30.48/−68.58 −32.61/−68.46, −32.54/−72.35	41–94	DDE/DDE	P	Marot et al. (2013)	L	19

Table A1
Continued

Slab	Region	Coordinates	Depth [km]	Mech UP/LP	660	Source	Data	No.
Izu-Bonin/Marianas	Marianas	23.54/141.51, 16.48/144.78 16.22/148.34, 23.60/147.40	81–272	DDC/DDE	P	Samowitz and Forsyth (1981)	T	20
	Marianas	18.87/145.06, 17.97/145.19 18.17/147.63, 19.09/147.56	82–297	–	P	Shiobara et al. (2010)	L	21
	Izu-Bonin	28.29/140.51, 26.38/140.60 26.39/143.07, 28.35/142.88	71–195	–	R	Nakata et al. (2019)	L	22
Solomon Islands	New Britain	−5.04/150.87, −5.68/151.58 −5.15/152.06, −4.69/151.39	63–164	Other/DDE	R	McGuire and Wiens (1995)	T	23
Ryukyu	NE Taiwan	25.69/121.52, 25.61/122.99 23.34/122.93, 23.63/121.11	41–126	DDE/DDE	N	Kao and Rau (1999)	L	24
	Kanto	36.30/138.74, 36.86/139.98 35.69/140.74, 35.02/139.40	36–87	DDC/DDE	N	Seno et al. (2001)	L	25
	Kyushu	32.57/130.55, 32.11/132.13 30.83/131.11, 31.33/130.04	64–138	Other/DDE	N	Nakajima (2019)	L	26
Cascadia	Mendocino	40.85/−125.60, 40.89/−123.73 40.11/−123.65, 40.13/−125.51	16–29	Other/other	N	Smith et al. (1993) Wang and Rogers (1994)	L	27
Tonga-Kermadec-NZ	Tonga	−26.02/179.24, −27.97/−175.54 −17.21/−171.10, −15.40/−175.93	60–162	DDC/DDE	P	Kawakatsu (1985)	T	28
	Tonga	−16.39/−177.29, −18.34/−173.09 −23.13/−175.16, −21.54/−178.89	90–273	DDC/DDE	P	Wei et al. (2017)	L	29
	New Zealand	−40.94/173.80, −40.39/174.77 −41.02/175.99, −41.99/174.40	49–79	DDE/DDE	N	Robinson (1986)	L	30
	New Zealand	−38.48/176.66, −39.31/178.14 −37.88/179.93, −37.01/178.50	46–80	DDE/DDE	N	McGinty et al. (2000)	L	31
	New Zealand	−39.52/174.13, −41.16/176.46 −42.73/174.46, −41.06/172.17	49–100	DDE/DDE	N	McGinty et al. (2000)	L	32
	New Zealand	−36.09/176.98, −37.76/179.90 −42.93/174.04, −41.18/170.85	51–176	–	N	Reyners et al. (2011)	L	33
	New Zealand	−40.22/173.96, −40.64/175.52 −41.70/174.12, −41.13/173.20	49–134	DDE/DDC	N	Evanzia et al. (2019)	L	34
Vanuatu	Vanuatu	−16.39/166.80, −18.12/167.49 −17.69/168.80, −16.02/168.14	29–81	DDC/DDE	R	Prévot et al. (1994)	L	35
Indonesia	Java	−7.12/109.57, −7.52/112.04 −9.84/111.52, −9.34/109.27	38–138	–	P	Koulakov et al. (2007)	L	36
	Sumatra	5.92/92.84, 2.96/94.78 5.11/97.28, 7.53/95.28	?	–	R	Qin and Singh (2015)	T	37

Note. DDE, downdip extensive focal mechanisms; DDC, downdip compressive focal mechanisms; N/R/P, slab does not reach/reaches but does not penetrate/penetrates the 660; L/T/G, study based on local/teleseismic/global data.

Table A2
Locations of Double Seismic Zones Postulated in Literature (Global Studies)

Study	Slab	Region	Coordinates	Mech UP/LP	660	Data	No.
Brudzinski et al. (2007)	Alaska	A1	54.37/−153.85, 56.53/−149.61, 59.26/−154.22, 57.09/−158.78	–	R	G	1
	Aleutian	A2	57.33/−147.57, 58.87/−145.81, 60.68/−152.21, 59.14/−154.06	–	R	G	
		A3	52.07/−164.69, 54.68/−156.77, 57.94/−159.73, 55.33/−168.33	–	R	G	
		A4	50.31/−180.83, 50.31/−177.17, 54.08/−177.01, 54.08/−180.99	–	N	G	
		A5	50.62/−172.83, 51.97/−166.88, 55.50/−168.85, 54.14/−175.31	–	R	G	
	Japan-Kuril-Kamchatka	K1	58.60/152.90, 53.71/148.78, 51.99/154.76, 56.88/158.70	–	P	G	
		K2	50.25/142.07, 48.80/139.60, 45.94/143.35, 47.39/145.69	–	R	G	
		J1	40.32/132.77, 38.08/132.77, 37.98/137.64, 40.23/137.64	–	R	G	
	Central America/ South America	C1	15.27/−96.48, 13.83/−94.34, 16.91/−92.06, 18.36/−94.22	–	P	G	
		C2	13.97/−94.42, 12.73/−92.60, 15.82/−90.33, 17.05/−92.17	–	P	G	
		N1	−3.26/−82.27, −12.20/−80.67, −11.53/−76.93, −2.59/−78.52	–	P	G	
		N2	−32.65/−73.23, −36.28/−74.01, −36.86/−69.47, −33.23/−68.69	DDE/DDE	P	G	
		N3	−14.17/−77.64, −17.47/−74.20, −14.79/−71.48, −11.48/−74.88	–	P	G	
		N4	−28.32/−72.71, −32.88/−72.71, −32.81/−68.32, −28.26/−68.32	–	P	G	
		N5	−21.67/−71.75, −27.15/−71.44, −26.90/−67.30, −21.42/−67.62	–	P	G	
	Izu-Bonin/Marianas	I1	33.76/131.86, 31.31/132.92, 32.54/137.20, 34.99/136.12	–	R	G	
		I2	29.88/132.95, 28.19/133.66, 29.43/137.77, 31.12/137.06	–	R	G	
		M1	19.12/143.80, 16.82/144.23, 17.44/148.15, 19.74/147.72	–	P	G	
		M2	15.80/144.26, 14.43/143.06, 11.98/146.03, 13.36/147.22	–	N	G	
	Solomon Is./ Ryukyu/Tonga-Kermandec-NZ	B1	−7.21/151.79, −6.08/153.42, −2.98/151.25, −4.12/149.62	–	R	G	
		R1	22.82/121.87, 22.82/123.73, 26.59/123.76, 26.59/121.84	–	N	G	
		Z1	−35.81/171.94, −39.33/168.22, −41.70/171.92, −38.19/175.77	–	N	G	
		T1	−18.28/179.54, −20.93/177.92, −22.79/181.42, −20.14/183.06	–	P	G	
		T2	−23.15/177.20, −25.19/176.81, −25.79/180.90, −23.76/181.30	–	P	G	
	Vanuatu/Indonesia	V1	−15.18/166.09, −16.79/165.94, −17.09/169.86, −15.47/170.01	–	R	G	
		S1	0.79/96.46, −1.20/97.85, 0.97/100.94, 2.96/99.55	–	P	G	
		S2	2.79/95.06, 0.80/96.45, 2.97/99.55, 4.95/98.15	–	R	G	
		S3	−3.31/99.25, −5.30/100.65, −3.13/103.75, −1.14/102.35	–	P	G	
		S4	−8.93/104.86, −10.39/108.20, −6.94/109.73, −5.48/106.42	Other/DDE	P	G	
		S5	−6.18/118.78, −5.46/114.69, −9.18/114.00, −9.90/118.13	–	P	G	
	Philippines	P1	12.04/121.23, 8.83/122.42, 10.10/126.05, 13.32/124.85	–	N	G	
		P2	8.65/121.95, 6.03/122.91, 7.31/126.50, 9.93/125.53	DDC/DDE	N	G	
Florez and Prieto (2019)	Alaska-Aleutian	AK1	48.64/−172.65, 55.34/−173.60, 55.03/−179.40, 48.33/−178.45	–	R	G	2
		AK2	60.36/−148.06, 62.11/−154.38, 59.00/−157.65, 57.25/−151.90	–	R	G	
		AK3	51.09/181.51, 52.58/181.51, 52.58/175.69, 51.09/175.69	–	N	G	
	Japan-Kuril-Kamchatka	KR1	50.64/161.12, 53.92/156.62, 51.61/152.34, 48.34/156.63	–	P	G	
		KR2	48.16/157.08, 50.73/153.13, 48.19/149.41, 45.62/153.17	–	P	G	
		KR3	41.31/151.16, 48.58/146.34, 47.06/141.87, 39.79/146.56	–	R	G	
		JP1	40.02/144.66, 40.82/138.73, 37.28/138.07, 36.49/143.72	–	R	G	

Table A2
Continued

Study	Slab	Region	Coordinates	Mech UP/LP	660	Data	No.
	Central America	CA1	13.27/−93.55, 16.83/−90.97, 18.89/−94.03, 15.33/−96.63	−	P	G	
		CA2	12.05/−90.30, 14.04/−88.87, 16.10/−91.90, 14.11/−93.34	−	P	G	
		CA3	9.35/−88.02, 13.65/−84.95, 15.71/−87.95, 11.42/−91.05	−	P	G	
	South America	SA1	−10.33/−78.82, −7.13/−71.87, −3.88/−73.42, −7.08/−80.32	−	P	G	
		SA2	−19.17/−73.51, −14.11/−69.08, −11.80/−71.96, −16.86/−76.34	−	P	G	
		SA3	−23.69/−70.37, −22.80/−65.83, −19.28/−66.68, −20.17/−71.12	−	P	G	
	Izu-Bonin/Marianas	IB1	36.07/142.49, 35.28/136.96, 31.74/137.83, 32.54/143.13	−	R	G	
		IB2	29.58/144.58, 28.10/136.62, 24.59/137.58, 26.07/145.29	−	R	G	
		IB3	25.25/144.56, 21.56/140.38, 18.97/143.11, 22.67/147.21	−	P	G	
		MR1	20.69/146.03, 20.43/144.51, 16.89/145.18, 17.14/146.67	−	P	G	
		MR2	13.23/147.17, 16.09/145.02, 13.98/142.04, 11.11/144.17	−	N	G	
	Solomon Islands	NB1	−7.34/148.67, −5.56/149.33, −4.33/145.93, −6.11/145.28	−	R	G	
		NB2	−7.04/151.74, −4.05/151.22, −4.68/147.65, −7.66/148.18	−	R	G	
		NB3	−4.82/153.79, −3.36/152.94, −5.16/149.81, −6.62/150.66	−	R	G	
		NB4	−5.90/155.71, −5.14/155.85, −4.51/152.29, −5.28/152.15	−	R	G	
		NB5	−8.66/155.84, −6.89/157.34, −4.58/154.56, −6.34/153.07	−	R	G	
	Tonga-Kermandec-NZ	TO1	−16.82/−171.51, −15.31/−174.89, −18.56/−176.52, −20.08/−173.08	−	P	G	
		TO2	−20.30/−173.07, −18.16/−177.00, −21.27/−178.97, −23.41/−174.95	−	P	G	
		TO3	−27.63/−172.44, −25.60/−180.38, −29.05/−181.63, −31.08/−173.43	−	P	G	
	Indonesia	SU1	4.14/91.57, 7.23/98.24, 10.48/96.73, 7.39/90.02	−	R	G	
		SU2	−2.41/96.57, 0.58/102.98, 3.83/101.47, 0.85/95.06	−	R	G	
		SU3	−7.68/102.13, −3.66/105.90, −1.21/103.26, −5.23/99.50	−	P	G	
		SN1	−11.27/108.61, −5.54/110.95, −4.20/107.58, −9.93/105.25	−	P	G	
		SN2	−11.22/115.04, −7.30/115.74, −6.67/112.16, −10.59/111.46	−	P	G	
		SN3	−10.55/120.82, −6.74/120.82, −6.74/117.18, −10.55/117.18	−	P	G	

Note. DDE, downdip extensive focal mechanisms; DDC, downdip compressive focal mechanisms; N/R/P, slab does not reach/reaches but does not penetrate/penetrates the 660; L/T/G, study based on local/teleseismic/global data as in Table A1.

Data Availability Statement

Data on observations and focal mechanisms of double seismic zones were taken from the studies listed in Tables A1 and A2. Slab geometry data were retrieved from slab2 (Hayes et al., 2018), accessed at https://www.sciencebase.gov/catalog/item/5aa1b00ee4b0b1c392e86467. Earthquake locations and mechanisms for Northern Chile (shown in Figure 12) were taken from Sippl et al. (2018) and Sippl et al. (2019), those for NE Japan (Figure 13) from Kita et al. (2010).

References

Abers, G. A. (1992). Relationship between shallow- and intermediate-depth seismicity in the eastern Aleutian subduction zone. *Geophysical Research Letters*, *19*(20), 2019–2022. https://doi.org/10.1029/92gl02060

Alpert, L. A., Becker, T. W., & Bailey, I. W. (2010). Global slab deformation and centroid moment tensor constraints on viscosity. *Geochemistry, Geophysics, Geosystems*, *11*(12), 1–22. https://doi.org/10.1029/2010GC003301

Arnulf, A. F., Bassett, D., Harding, A. J., Kodaira, S., Nakanishi, A., & Moore, G. (2022). Upper-plate controls on subduction zone geometry, hydration and earthquake behaviour. *Nature Geoscience*, *15*(2), 143–148. https://doi.org/10.1038/s41561-021-00879-x

Austrheim, H. (1987). Eclogitization of lower crustal granulites by fluid migration through shear zones. *Earth and Planetary Science Letters*, *81*(2–3), 221–232. https://doi.org/10.1016/0012-821X(87)90158-0

Babeyko, A., & Sobolev, S. V. (2008). High-resolution numerical modeling of stress distribution in visco-elasto-plastic subducting slabs. *Lithos*, *103*(1–2), 205–216. https://doi.org/10.1016/j.lithos.2007.09.015

Bailey, I. W., Alpert, L. A., Becker, T. W., & Miller, M. S. (2012). Co-seismic deformation of deep slabs based on summed CMT data. *Journal of Geophysical Research*, *117*(4), 1–19. https://doi.org/10.1029/2011JB008943

Bedford, J., Moreno, M., Deng, Z., Oncken, O., Schurr, B., John, T., et al. (2020). Months-long thousand-kilometre-scale wobbling before great subduction earthquakes. *Nature*, *580*(7805), 628–635. https://doi.org/10.1038/s41586-020-2212-1

Bellahsen, N., Faccenna, C., & Funiciello, F. (2005). Dynamics of subduction and plate motion in laboratory experiments: Insights into the "plate tectonics" behavior of the Earth. *Journal of Geophysical Research*, *110*(1), 1–15. https://doi.org/10.1029/2004JB002999

Bessat, A., Duretz, T., Hetényi, G., Pilet, S., & Schmalholz, S. M. (2020). Stress and deformation mechanisms at a subduction zone: Insights from 2-D thermomechanical numerical modelling. *Geophysical Journal International*, *221*(3), 1605–1625. https://doi.org/10.1093/gji/ggaa092

Bloch, W., John, T., Kummerow, J., Salazar, P., Krüger, O. S., & Shapiro, S. A. (2018). Watching dehydration: Seismic indication for transient fluid pathways in the oceanic mantle of the subducting nazca slab. *Geochemistry, Geophysics, Geosystems*, *19*(9), 3189–3207. https://doi.org/10.1029/2018GC007703

Bloch, W., Schurr, B., Kummerow, J., Salazar, P., & Shapiro, S. A. (2018). From slab coupling to slab pull: Stress segmentation in the subducting nazca plate. *Geophysical Research Letters*, *45*(11), 5407–5416. https://doi.org/10.1029/2018GL078793

Bostock, M. G., Hyndman, R. D., Rondenay, S., & Peacock, S. M. (2002). An inverted continental moho and serpentinization of the forearc mantle. *Nature*, *417*(6888), 536–538. https://doi.org/10.1038/417536a

Bouih, M., Panet, I., Remy, D., Longuevergne, L., & Bonvalot, S. (2022). Deep mass redistribution prior to the 2010 Mw 8.8 Maule (Chile) Earthquake revealed by GRACE satellite gravity. *Earth and Planetary Science Letters*, *584*, 117465. https://doi.org/10.1016/j.epsl.2022.117465

Brudzinski, M. R., Thurber, C. H., Hacker, B. R., & Engdahl, E. R. (2007). Global prevalence of double benioff zones. *Science*, *316*(5830), 1472–1474. https://doi.org/10.1126/science.1139204

Buffett, B. A. (2006). Plate force due to bending at subduction zones. *Journal of Geophysical Research*, *111*(9), 1–9. https://doi.org/10.1029/2006JB004295

Buffett, B. A., & Heuret, A. (2011). Curvature of subducted lithosphere from earthquake locations in the Wadati-Benioff zone. *Geochemistry, Geophysics, Geosystems*, *12*(6), 1–13. https://doi.org/10.1029/2011GC003570

Cabrera, L., Ruiz, S., Poli, P., Contreras-Reyes, E., Osses, A., & Mancini, R. (2021). Northern Chile intermediate-depth earthquakes controlled by plate hydration. *Geophysical Journal International*, *226*(1), 78–90. https://doi.org/10.1093/gji/ggaa565

Cai, C., Wiens, D. A., Shen, W., & Eimer, M. (2018). Water input into the Mariana subduction zone estimated from ocean-bottom seismic data. *Nature*, *563*(7731), 389–392. https://doi.org/10.1038/s41586-018-0655-4

Capitanio, F. A., Morra, G., & Goes, S. (2009). Dynamics of plate bending at the trench and slab-plate coupling. *Geochemistry, Geophysics, Geosystems*, *10*(4), Q04002. https://doi.org/10.1029/2008GC002348

Chen, P. F., Bina, C., & Okal, E. (2004). A global survey of stress orientations in subducting slabs as revealed by intermediate-depth earthquakes. *Geophysical Journal International*, *159*(2), 721–733. https://doi.org/10.1111/j.1365-246X.2004.02450.x

Comte, D., Dorbath, L., Pardo, M., Monfret, T., Haessler, H., Rivera, L., et al. (1999). A double-layered seismic zone in Arica, northern Chile. *Geophysical Research Letters*, *26*(13), 1965–1968. https://doi.org/10.1029/1999GL900447

Comte, D., & Suárez, G. (1994). An inverted double seismic zone in Chile: Evidence for phase transformation in the subducted slab. *Science*, *263*(5144), 212–215. https://doi.org/10.1126/science.263.5144.212

Craig, T. J., Copley, A., & Jackson, J. (2014). A reassessment of outer-rise seismicity and its implications for the mechanics of oceanic lithosphere. *Geophysical Journal International*, *197*(1), 63–89. https://doi.org/10.1093/gji/ggu013

Craig, T. J., Methley, P., & Sandiford, D. (2022). Imbalanced moment release within subducting plates during initial bending and (un) bending. *Journal of Geophysical Research*, *40*(3). https://doi.org/10.1029/2021JB023658

Dielforder, A. (2017). Constraining the strength of megathrusts from fault geometries and application to the Alpine collision zone. *Earth and Planetary Science Letters*, *474*, 49–58. https://doi.org/10.1016/j.epsl.2017.06.021

Dielforder, A., Hetzel, R., & Oncken, O. (2020). Megathrust shear force controls mountain height at convergent plate margins. *Nature*, *582*(7811), 225–229. https://doi.org/10.1038/s41586-020-2340-7

Dorbath, C., Gerbault, M., Carlier, G., & Guiraud, M. (2008). Double seismic zone of the Nazca plate in northern Chile: High-resolution velocity structure, petrological implications, and thermomechanical modeling. *Geochemistry, Geophysics, Geosystems*, *9*(7). https://doi.org/10.1029/2008GC002020

Engdahl, E. R., & Scholz, C. H. (1977). A double benioff zone beneath the central Aleutians: An (un) bending of the lithosphere. *Geophysical Research Letters*, *4*(10), 473–476. https://doi.org/10.1029/GL004i010p00473

Erdos, Z., Huismans, R. S., Faccenna, C., & Wolf, S. G. (2021). The role of subduction interface and upper plate strength on back-arc extension: Application to mediterranean back-arc basins. *Tectonics*, *40*(8). https://doi.org/10.1029/2021TC006795

Evanzia, D., Lamb, S., Savage, M. K., & Stern, T. A. (2019). Illumination of deformation by bending stresses and slab pull within the southern hikurangi double benioff zone. *New Zealand Journal of Geology and Geophysics*, *62*(1), 111–120. https://doi.org/10.1080/00288306.2018.1532439

Faccenda, M., Gerya, T. V., Mancktelow, N. S., & Moresi, L. (2012). Fluid flow during slab (un) bending and dehydration: Implications for intermediate-depth seismicity, slab weakening and deep water recycling. *Geochemistry, Geophysics, Geosystems*, *13*(1), Q01010. https://doi.org/10.1029/2011GC003860

Faccenda, M., & Mancktelow, N. S. (2010). Fluid flow during (un) bending: Implications for slab hydration, intermediate-depth earthquakes and deep fluid subduction. *Tectonophysics*, *494*(1–2), 149–154. https://doi.org/10.1016/j.tecto.2010.08.002

Ferrand, T., Hilairet, N., Incel, S., Deldicque, D., Labrousse, L., Gasc, J., et al. (2017). Dehydration-driven stress transfer triggers intermediate-depth earthquakes. *Nature Communications*, *8*, 1–11. https://doi.org/10.1038/ncomms15247

Florez, M. A., & Prieto, G. A. (2019). Controlling factors of seismicity and geometry in double seismic zones. *Geophysical Research Letters*, *46*(8), 4174–4181. https://doi.org/10.1029/2018GL081168

Forsyth, D. W., & Uyeda, S. (1975). On the driving forces of plate tectonics. *Geophysical Journal of the Royal Astronomical Society*, *43*(3), 163–200. https://doi.org/10.1111/j.1365-246X.1975.tb04143.x

Fourel, L., Goes, S., & Morra, G. (2014). The role of elasticity in slab bending. *Geochemistry, Geophysics, Geosystems*, *15*(11), 4507–4525. https://doi.org/10.1002/2014GC005535

Frehner, M. (2011). The neutral lines in buckle folds. *Journal of Structural Geology*, *33*(10), 1501–1508. https://doi.org/10.1016/j.jsg.2011.07.005

Fujita, K., & Kanamori, H. (1981). Double seismic zones and stresses of intermediate depth earthquakes. *Geophysical Journal of the Royal Astronomical Society*, *66*(1), 131–156. https://doi.org/10.1111/j.1365-246X.1981.tb05950.x

Funiciello, F., Morra, G., Regenauer-Lieb, K., & Giardini, D. (2003). Dynamics of retreating slabs: 1. Insights from two-dimensional numerical experiments. *Journal of Geophysical Research*, *108*(B4), 2206. https://doi.org/10.1029/2001jb000898

Gamage, S. S., Umino, N., Hasegawa, A., & Kirby, S. (2009). Offshore double-planed shallow seismic zone in the NE Japan forearc region revealed by sP depth phases recorded by regional networks. *Geophysical Journal International*, *178*(1), 195–214. https://doi.org/10.1111/j.1365-246X.2009.04048.x

Gao, X., & Wang, K. (2014). Strength of stick-slip and creeping subduction megathrusts from heat flow observations. *Science*, *345*(6200), 1038–1041. https://doi.org/10.1126/science.1255487

Garcia, E. S. M., Sandwell, D. T., & Bassett, D. (2019). Outer trench slope flexure and faulting at Pacific basin subduction zones. *Geophysical Journal International*, *218*(1), 708–728. https://doi.org/10.1093/gji/ggz155

Geersen, J., Sippl, C., & Harmon, N. (2022). Impact of bending-related faulting and oceanic-plate topography on slab hydration and intermediate-depth seismicity. *Geosphere*, *18*(2), 562–584. https://doi.org/10.1130/GES02367.1

Goes, S., Agrusta, R., van Hunen, J., & Garel, F. (2017). Subduction-transition zone interaction: A review. *Geosphere*, *13*(3), 644–664. https://doi.org/10.1130/GES01476.1

Gorbatov, A., Suarez, G., Kostoglodov, V., & Gordeev, E. I. (1994). A double-planed seismic zone in Kamchatka from local and teleseismic data. *Geophysical Research Letters*, *21*(16), 1675–1678. https://doi.org/10.1029/94GL01593

Grevemeyer, I., Ranero, C. R., & Ivandic, M. (2018). Structure of oceanic crust and serpentinization at subduction trenches. *Geosphere*, *14*(2), 395–418. https://doi.org/10.1130/GES01537.1

Hacker, B. R., Abers, G. A., & Peacock, S. M. (2003). Subduction factory 1. Theoretical mineralogy, densities, seismic wave speeds, and H_2O contents. *Journal of Geophysical Research*, *108*(B1), 2029. https://doi.org/10.1029/2001jb001127

Hacker, B. R., Peacock, S. M., Abers, G. A., & Holloway, S. D. (2003). Subduction factory 2. Are intermediate-depth earthquakes in subducting slabs linked to metamorphic dehydration reactions? *Journal of Geophysical Research*, *108*(B1). https://doi.org/10.1029/2001JB001129

Hasegawa, A., Umino, N., & Takagi, A. (1978). Double-planed structure of the deep seismic zone in the northeastern Japan arc. *Tectonophysics*, *47*(1–2), 43–58. https://doi.org/10.1016/0040-1951(78)90150-6

Hayes, G. P., Moore, G., Portner, D. E., Hearne, M., Flamme, H., Furtney, M., & Smoczyk, G. M. (2018). Slab2, a comprehensive subduction zone geometry model. *Science*, *362*(6410), 58–61. https://doi.org/10.1126/science.aat4723

Hayes, G. P., Wald, D. J., & Johnson, R. L. (2012). Slab1.0: A three-dimensional model of global subduction zone geometries. *Journal of Geophysical Research*, *117*(1), 1–15. https://doi.org/10.1029/2011JB008524

Hu, J., & Gurnis, M. (2020). Subduction duration and slab dip. *Geochemistry, Geophysics, Geosystems*, *21*(4), 1–34. https://doi.org/10.1029/2019gc008862

Hudnut, K. W., & Taber, J. J. (1987). Transition from double to single Wadati-Benioff seismic zone in the Shumagin Islands, Alaska. *Geophysical Research Letters*, *14*(2), 143–146. https://doi.org/10.1029/GL014i002p00143

Hunter, J., & Watts, A. B. (2016). Gravity anomalies, flexure and mantle rheology seaward of circum-Pacific trenches. *Geophysical Journal International*, *207*(1), 288–316. https://doi.org/10.1016/B978-0-323-60984-5.00062-7

Hunter, J. D. (2007). Matplotlib: A 2D graphics environment. *Computing in Science & Engineering*, *9*(3), 90–95. https://doi.org/10.1109/MCSE.2007.55

Igarashi, T., Matsuzawa, T., Umino, N., & Hasegawa, A. (2001). Spatial distribution of focal mechanisms for interplate and intraplate earthquakes associated with the subducting Pacific plate beneath the northeastern Japan arc: A triple-planed deep seismic zone. *Journal of Geophysical Research*, *106*(B2), 2177–2191. https://doi.org/10.1029/2000jb900386

Incel, S., Hilairet, N., Labrousse, L., John, T., Deldicque, D., Ferrand, T., et al. (2017). Laboratory earthquakes triggered during eclogitization of lawsonite-bearing blueschist. *Earth and Planetary Science Letters*, *459*, 320–331. https://doi.org/10.1016/j.epsl.2016.11.047

Isacks, B. L., & Barazangi, M. (1977). Geometry of benioff zones: Lateral segmentation and downwards bending of the subducted lithosphere. *Island Arc, Deep Sea Trenches and Back-Arc Basins; Maurice Ewing Series*, *1*, 99–113.

Isacks, B. L., & Molnar, P. (1969). Mantle earthquake mechanisms and the sinking of the lithosphere. *Nature*, *223*(5211), 1121–1124. https://doi.org/10.1038/2231121a0

Isacks, B. L., & Molnar, P. (1971). Distribution of stresses in the descending lithosphere from a global survey of focal-mechanism solutions of mantle earthquakes. *Reviews of Geophysics*, *9*(1), 103–174. https://doi.org/10.1029/RG009i001p00103

John, T., Medvedev, S., Rüpke, L. H., Andersen, T. B., Podladchikov, Y., & Austrheim, H. (2009). Generation of intermediate-depth earthquakes by self-localizing thermal runaway. *Nature Geoscience*, *2*(2), 137–140. https://doi.org/10.1038/ngeo419

Jung, H., Green, H., & Dobrzhinetskaya, L. F. (2004). Intermediate-depth earthquake faulting by dehydration embrittlement with negative volume change. *Nature*, *428*(6982), 545–549. https://doi.org/10.1038/nature02412

Kaatz, L., Zertani, S., Moulas, E., John, T., Labrousse, L., Schmalholz, S. M., & Andersen, T. B. (2021). Widening of hydrous shear zones during incipient eclogitization of metastable dry and rigid lower crust–holsnøy, Western Norway. *Tectonics*, *40*(3), 1–19. https://doi.org/10.1029/2020TC006572

Kao, H., & Chen, W. P. (1995). Transition from interplate slip to double seismic zone along the Kuril-Kamchatka Arc. *Journal of Geophysical Research*, *100*(B7), 9881–9903. https://doi.org/10.1029/95JB00239

Kao, H., & Rau, R.-J. (1999). Detailed structures of the subducted Philippine sea plate beneath northeast Taiwan: A new type of double seismic zone. *Journal of Geophysical Research*, *104*(B1), 1015–1033. https://doi.org/10.1029/1999JB900356

Kawakatsu, H. (1985). Double seismic zone in Tonga. *Nature*, *316*(6023), 53–55. https://doi.org/10.1038/316053a0

Kawakatsu, H. (1986). Double seismic zones: Kinematics. *Journal of Geophysical Research*, *91*(B5), 4811–4825. https://doi.org/10.1029/jb091ib05p04811

Kirby, S., Engdahl, E. R., & Denlinger, R. (1996). Intermediate-depth intraslab earthquakes and arc volcanism as physical expressions of crustal and uppermost mantle metamorphism in subducting slabs. *Geophysical Monograph Series*, *96*, 195–214. https://doi.org/10.1029/GM096p0195

Kita, S., Okada, T., Hasegawa, A., Nakajima, J., & Matsuzawa, T. (2010). Existence of interplane earthquakes and neutral stress boundary between the upper and lower planes of the double seismic zone beneath Tohoku and Hokkaido, northeastern Japan. *Tectonophysics*, *496*(1–4), 68–82. https://doi.org/10.1016/j.tecto.2010.10.010

Kita, S., Okada, T., Nakajima, J., Matsuzawa, T., & Hasegawa, A. (2006). Existence of a seismic belt in the upper plane of the double seismic zone extending in the along-arc direction at depths of 70-100 km beneath NE Japan. *Geophysical Research Letters*, *33*(24), L24310. https://doi.org/10.1029/2006GL028239

Korenaga, J. (2017). On the extent of mantle hydration caused by plate bending. *Earth and Planetary Science Letters*, *457*, 1–9. https://doi.org/10.1016/j.epsl.2016.10.011

Koulakov, I., Bohm, M., Asch, G., Lühr, B. G., Manzanares, A., Brotopuspito, K. S., et al. (2007). P and S velocity structure of the crust and the upper mantle beneath central Java from local tomography inversion. *Journal of Geophysical Research*, *112*(8), 1–19. https://doi.org/10.1029/2006JB004712

Lamb, S. (2006). Shear stresses on megathrusts: Implications for mountain building behind subduction zones. *Journal of Geophysical Research*, *111*(B7), B07401. https://doi.org/10.1029/2005jb003916

Lambert, V., Lapusta, N., & Perry, S. (2021). Propagation of large earthquakes as self-healing pulses or mild cracks. *Nature*, *591*(7849), 252–258. https://doi.org/10.1038/s41586-021-03248-1

Lefeldt, M., Grevemeyer, I., Goßler, J., & Bialas, J. (2009). Intraplate seismicity and related mantle hydration at the Nicaraguan trench outer rise. *Geophysical Journal International*, *178*(2), 742–752. https://doi.org/10.1111/j.1365-246X.2009.04167.x

Li, C., van der Hilst, R. D., Engdahl, E. R., & Burdick, S. (2008). A new global model for P wave speed variations in Earth's mantle. *Geochemistry, Geophysics, Geosystems*, *9*(5), Q05018. https://doi.org/10.1029/2007GC001806

Manea, V. C., Marta, P. G., & Manea, M. (2012). Chilean flat slab subduction controlled by overriding plate thickness and trench rollback. *Geology*, *40*(1), 35–38. https://doi.org/10.1130/G32543.1

Marot, M., Monfret, T., Pardo, M., Ranalli, G., & Nolet, G. (2013). A double seismic zone in the subducting juan fernandez ridge of the nazca plate (32°S), central Chile. *Journal of Geophysical Research*, *118*(7), 3462–3475. https://doi.org/10.1002/jgrb.50240

McGinty, P., Reyners, M., & Robinson, R. (2000). Stress directions in the shallow part of the Hikurangi subduction zone, New Zealand, from the inversion of earthquake first motions. *Geophysical Journal International*, *142*(2), 339–350. https://doi.org/10.1046/j.1365-246x.2000.00155.x

McGuire, J. J., & Wiens, D. A. (1995). A double seismic zone in New Britain and the morphology. *Geophysical Research Letters*, *22*(15), 1965–1968. https://doi.org/10.1029/95gl01806

Medvedev, S. (2016). Understanding lithospheric stresses: Systematic analysis of controlling mechanisms with applications to the African Plate. *Geophysical Journal International*, *207*(1), 393–413. https://doi.org/10.1093/gji/ggw241

Nakajima, J. (2019). Revisiting intraslab earthquakes beneath Kyushu, Japan: Effect of ridge subduction on seismogenesis. *Journal of Geophysical Research: Solid Earth*, *124*(8), 8660–8678. https://doi.org/10.1029/2019JB017869

Nakajima, J., Uchida, N., Shiina, T., Hasegawa, A., Hacker, B. R., & Kirby, S. (2013). Intermediate-depth earthquakes facilitated by eclogitization-related stresses. *Geology*, *41*(6), 659–662. https://doi.org/10.1130/G33796.1

Nakata, K., Kobayashi, A., Katsumata, A., Hirose, F., Nishimiya, T., Kimura, K., et al. (2019). Double seismic zone and seismicity in the mantle wedge beneath the Ogasawara Islands identified by an ocean bottom seismometer observation. *Earth Planets and Space*, *71*(1), 29. https://doi.org/10.1186/s40623-019-1012-z

Obayashi, M., Yoshimitsu, J., Nolet, G., Fukao, Y., Shiobara, H., Sugioka, H., et al. (2013). Finite frequency whole mantle P wave tomography: Improvement of subducted slab images. *Geophysical Research Letters*, *40*(21), 5652–5657. https://doi.org/10.1002/2013GL057401

Peacock, S. M. (2001). Are the lower planes of double seismic zones caused by serpentine dehydration in subducting oceanic mantle? *Geology*, *29*(4), 299–302. https://doi.org/10.1130/0091-7613(2001)029<0299:ATLPOD>2.0.CO;2

Plümper, O., John, T., Podladchikov, Y. Y., Vrijmoed, J. C., & Scambelluri, M. (2017). Fluid escape from subduction zones controlled by channel-forming reactive porosity. *Nature Geoscience*, *10*(2), 150–156. https://doi.org/10.1038/ngeo2865

Plümper, O., Røyne, A., Magrasó, A., & Jamtveit, B. (2012). The interface-scale mechanism of reaction-induced fracturing during serpentinization. *Geology*, *40*(12), 1103–1106. https://doi.org/10.1130/G33390.1

Portner, D. E., & Hayes, G. P. (2018). Incorporating teleseismic tomography data into models of upper mantle slab geometry. *Geophysical Journal International*, *215*(1), 325–332. https://doi.org/10.1093/gji/ggy279

Prévot, R., Chatelain, J. L., Roecker, S. W., & Grasso, J. â. (1994). A shallow double seismic zone beneath the central new hebrides (Vanuatu): Evidence for fragmentation and accretion of the descending plate? *Geophysical Research Letters*, *21*(19), 2159–2162. https://doi.org/10.1029/94GL01961

Qin, Y., & Singh, S. C. (2015). Seismic evidence of a two-layer lithospheric deformation in the Indian Ocean. *Nature Communications*, *6*, 1–12. https://doi.org/10.1038/ncomms9298

Ranero, C. R., & Sallarès, V. (2004). Geophysical evidence for hydration of the crust and mantle of the Nazca plate during bending at the north Chile trench. *Geology*, *32*(7), 549–552. https://doi.org/10.1130/G20379.1

Ranero, C. R., Villaseñor, A., Morgan, J. P., & Weinrebe, W. (2005). Relationship between bend-faulting at trenches and intermediate-depth seismicity. *Geochemistry, Geophysics, Geosystems*, *6*(12), Q12002. https://doi.org/10.1029/2005GC000997

Ratchkovsky, N. A., Pujol, J., & Biswas, N. N. (1997). Stress pattern in the double seismic zone beneath Cook Inlet, south-central Alaska. *Tectonophysics*, *281*(3–4), 163–171. https://doi.org/10.1016/S0040-1951(97)00042-5

Reyners, M., & Coles, K. S. (1982). Fine structure of the dipping seismic zone and subduction mechanics in the Shumagin Islands, Alaska. *Journal of Geophysical Research*, *87*(B1), 356–366. https://doi.org/10.1029/JB087iB01p00356

Reyners, M., Eberhart-Phillips, D., & Bannister, S. (2011). Tracking repeated subduction of the Hikurangi plateau beneath New Zealand. *Earth and Planetary Science Letters*, *311*(1–2), 165–171. https://doi.org/10.1016/j.epsl.2011.09.011

Ribe, N. M. (2001). Bending and stretching of thin viscous sheets. *Journal of Fluid Mechanics*, *433*, 135–160. https://doi.org/10.1017/S0022112000003360

Ribe, N. M. (2010). Bending mechanics and mode selection in free subduction: A thin-sheet analysis. *Geophysical Journal International*, *180*(2), 559–576. https://doi.org/10.1111/j.1365-246X.2009.04460.x

Rietbrock, A., & Waldhauser, F. (2004). A narrowly spaced double-seismic zone in the subducting Nazca plate. *Geophysical Research Letters*, *31*(10), L10608. https://doi.org/10.1029/2004GL019610

Robinson, R. (1986). Seismicity, structure and tectonics of the Wellington region, New Zealand. *Geophysical Journal of the Royal Astronomical Society*, *87*(2), 379–409. https://doi.org/10.1111/j.1365-246X.1986.tb06629.x

Samowitz, I. R., & Forsyth, D. W. (1981). Double seismic zone beneath the Mariana Island arc. *Journal of Geophysical Research*, *86*(B8), 7013–7021. https://doi.org/10.1029/JB086iB08p07013

Sandiford, D., Moresi, L., Sandiford, M., Farrington, R., & Yang, T. (2020). The fingerprints of flexure in slab seismicity. *Tectonics*, *39*(8), e2019TC005894. https://doi.org/10.1029/2019tc005894

Sandiford, D., Moresi, L., Sandiford, M., & Yang, T. (2019). Geometric controls on flat slab seismicity. *Earth and Planetary Science Letters*, *527*, 115787. https://doi.org/10.1016/j.epsl.2019.115787

Schellart, W. P. (2004). Quantifying the net slab pull force as a driving mechanism for plate tectonics. *Geophysical Research Letters*, *31*(7), L07611. https://doi.org/10.1029/2004GL019528

Seno, T., & Yamanaka, Y. (1996). Double seismic zones, compressional deep trench-outer rise events, and superplumes. In G. Bebout, D. Scholl, S. Kirby, & J. Platt (Eds.), *Subduction: Top to bottom; geophysical monograph series* (Vol. 96, pp. 347–355). AGU. https://doi.org/10.1029/GM096p0347

Seno, T., Zhao, D., Kobayashi, Y., & Nakamura, M. (2001). Dehydration of serpentinized slab mantle: Seismic evidence from southwest Japan. *Earth Planets and Space*, *53*(9), 861–871. https://doi.org/10.1186/BF03351683

Shiobara, H., Sugioka, H., Mochizuki, K., Oki, S., Kanazawa, T., Fukao, Y., & Suyehiro, K. (2010). Double seismic zone in the North Mariana region revealed by long-term ocean bottom array observation. *Geophysical Journal International*, *183*(3), 1455–1469. https://doi.org/10.1111/j.1365-246X.2010.04799.x

Simmons, N. A., Myers, S. C., Johannesson, G., & Matzel, E. (2012). LLNL-G3Dv3: Global P wave tomography model for improved regional and teleseismic travel time prediction. *Journal of Geophysical Research*, *117*(10), 1–28. https://doi.org/10.1029/2012JB009525

Sippl, C., Schurr, B., Asch, G., & Kummerow, J. (2018). Seismicity structure of the northern Chile forearc from >100, 000 double-difference relocated hypocenters. *Journal of Geophysical Research*, *123*(5), 4063–4087. https://doi.org/10.1002/2017jb015384

Sippl, C., Schurr, B., John, T., & Hainzl, S. (2019). Filling the gap in a double seismic zone: Intraslab seismicity in Northern Chile. *Lithos*, *346–347*, 105155. https://doi.org/10.1016/j.lithos.2019.105155

Slancova, A., Spicak, A., Hanuš, V., & Vaněk, J. (2000). How the state of stress varies in the Wadati-Benioff zone: Indications from focal mechanisms in the Wadati-Benioff zone beneath Sumatra and Java. *Geophysical Journal International*, *143*(3), 909–930. https://doi.org/10.1046/j.0956-540X.2000.01304.x

Smith, S. W., Knapp, J. S., & McPherson, R. C. (1993). Seismicity of the Gorda Plate, structure of the continental margin, and an eastward jump of the Mendocino triple junction. *Journal of Geophysical Research*, *98*(B5), 8153–8171. https://doi.org/10.1029/93JB00026

Sobolev, S. V., & Muldashev, I. A. (2017). Modeling seismic cycles of great megathrust earthquakes across the scales with focus at Postseismic phase. *Geochemistry, Geophysics, Geosystems*, *18*(12), 4387–4408. https://doi.org/10.1002/2017GC007230

Spakman, W., & Hall, R. (2010). Surface deformation and slab-mantle interaction during Banda arc subduction rollback. *Nature Geoscience*, *3*(8), 562–566. https://doi.org/10.1038/ngeo917

Syracuse, E., van Keken, P., Abers, G. A., Suetsugu, D., Bina, C., Inoue, T., & Jellinek, A. M. (2010). The global range of subduction zone thermal models. *Physics of the Earth and Planetary Interiors*, *183*(1–2), 73–90. https://doi.org/10.1016/j.pepi.2010.02.004

Turcotte, D. L., & Schubert, G. (2002). *Geodynamics*. Cambridge University Press.

van Zelst, I., Wollherr, S., Gabriel, A. A., Madden, E. H., & van Dinther, Y. (2019). Modeling megathrust earthquakes across scales: One-way coupling from geodynamics and seismic cycles to dynamic rupture. *Journal of Geophysical Research: Solid Earth*, *124*(11), 11414–11446. https://doi.org/10.1029/2019JB017539

Vassiliou, M. S., & Hager, B. H. (1988). Subduction zone earthquakes and stress in slabs. *Pure and Applied Geophysics*, *128*(3–4), 547–624. https://doi.org/10.1007/BF00874550

Wada, I., & Wang, K. (2009). Common depth of slab-mantle decoupling: Reconciling diversity and uniformity of subduction zones. *Geochemistry, Geophysics, Geosystems*, *10*(10), Q10009. https://doi.org/10.1029/2009GC002570

Wang, K. (2002). Unbending combined with dehydration embrittlement as a cause for double and triple seismic zones. *Geophysical Research Letters*, *29*(18), 1889–36-4. https://doi.org/10.1029/2002gl015441

Wang, K., Brown, L., Hu, Y., Yoshida, K., He, J., & Sun, T. (2019). Stable forearc stressed by a weak megathrust: Mechanical and geodynamic implications of stress changes caused by the M = 9 Tohoku-Oki earthquake. *Journal of Geophysical Research: Solid Earth*, *124*(6), 6179–6194. https://doi.org/10.1029/2018JB017043

Wang, K., & He, J. (1999). Mechanics of low-stress forearcs: Nankai and Cascadia. *Journal of Geophysical Research*, *104*(B7), 15191–15205. https://doi.org/10.1029/1999jb900103

Wang, K., & Rogers, G. C. (1994). An explanation for the double seismic layers north of the Mendocino Triple Junction. *Geophysical Research Letters*, *21*(2), 121–124. https://doi.org/10.1029/93GL03538

Wei, S. S., Ruprecht, P., Gable, S. L., Huggins, E. G., Ruppert, N. A., Gao, L., & Zhang, H. (2021). Along-strike variations in intermediate-depth seismicity and arc magmatism along the Alaska Peninsula. *Earth and Planetary Science Letters*, *563*, 116878. https://doi.org/10.1016/j.epsl.2021.116878

Wei, S. S., Wiens, D. A., van Keken, P., & Cai, C. (2017). Slab temperature controls on the Tonga double seismic zone and slab mantle dehydration. *Science Advances*, *3*(1), e1601755. https://doi.org/10.1126/sciadv.1601755

Wu, Y. M., Chang, C. H., Zhao, L., Teng, T. L., & Nakamura, M. (2008). A comprehensive relocation of earthquakes in Taiwan from 1991 to 2005. *Bulletin of the Seismological Society of America*, *98*(3), 1471–1481. https://doi.org/10.1785/0120070166

Yamasaki, T., & Seno, T. (2003). Double seismic zone and dehydration embrittlement of the subducting slab. *Journal of Geophysical Research*, *108*(B4), 2212. https://doi.org/10.1029/2002jb001918

Yuan, X., Sobolev, S. V., Kind, R., Oncken, O., Bock, G., Asch, G., et al. (2000). Subduction and collision processes in the Central Andes constrained by converted seismic phases. *Nature*, *408*(6815), 958–961. https://doi.org/10.1038/35050073

Zertani, S., John, T., Tilmann, F., Motra, H. B., Keppler, R., Andersen, T. B., & Labrousse, L. (2019). Modification of the seismic properties of subducting continental crust by eclogitization and deformation processes. *Journal of Geophysical Research: Solid Earth*, *124*(9), 9731–9754. https://doi.org/10.1029/2019JB017741

Zhan, Z. (2020). Mechanisms and implications of deep earthquakes. *Annual Review of Earth and Planetary Sciences*, *48*(1), 147–174. https://doi.org/10.1146/annurev-earth-053018-060314

Zhang, H., Wang, F., Myhill, R., & Guo, H. (2019). Slab morphology and deformation beneath Izu-Bonin. *Nature Communications*, *10*(1), 1310. https://doi.org/10.1038/s41467-019-09279-7